NOVEL EXTRINSIC AND INTRINSIC FACTORS MEDIATING OSTEOARTHRITIS

by

Kara A. Negrini

A Thesis

Submitted to the Faculty of Purdue University

In Partial Fulfillment of the Requirements for the degree of

Master of Science

Department of Basic Medical Sciences

West Lafayette, Indiana

May 2020

THE PURDUE UNIVERSITY GRADUATE SCHOOL
STATEMENT OF COMMITTEE APPROVAL

Dr. Dianne Little, Chair

Department of Basic Medical Sciences

Dr. Timothy Lescun

Department of Veterinary Clinical Sciences

Dr. Russell Main

Department of Basic Medical Sciences

Dr. Laurie Jaeger

Department of Basic Medical Sciences

Approved by:

Dr. Laurie Jaeger

ACKNOWLEDGMENTS

Thank you to the people who contributed to the initial portion of the Social Defeat study from Purdue University[1], Duke University[2] and North Carolina A&T State University[3]: Paula Sarmiento[1], Thomas Jenkins[1], Christopher Means[2], Lauren Thompson[3], Stephen Johnson[2], Ramona M. Rodriguiz[2], Cindy Nakatsu[1], and William C. Wetsel[2].

An additional special thank you to everyone who has supported me throughout this research: Dr. Dianne Little[1,2] who brought the study to Purdue University and advised me on this project, the MORE Lab for their support: Paula Sarmiento, Thomas Jenkins, and Abigail Green, and my family who supported me despite being 1000 miles away. I would also like to recognize Dr. Timothy Lescun, Dr. Russel Main, and Dr. Laurie Jaeger for being a part of my thesis committee.

I would like to acknowledge the following groups who helped with specific aspects of this thesis: Purdue University Imaging Facility, Eve Technologies Corporation, Purdue University Histology Research Laboratory, Purdue University Animal Disease and Diagnostic Laboratory, Purdue University Department of Veterinary Clinical Sciences and Large Animal Surgery Team, and Duke University IACUC.

We would also like to thank the funding that made this work possible: Department of Orthopaedic Surgery at Duke University, Department of Basic Medical Sciences at Purdue University, and the Purdue University Equine Research Advisory Board.

TABLE OF CONTENTS

LIST OF TABLES

LIST OF FIGURES

LIST OF ABBREVIATIONS

ACK	Ammonium-Chloride-Potassium
ASIC	Acid-Sensing Ion Channel
BDNF	Brain-Derived Neurotrophic Factor
BMA	Bone Microarchitecture Analysis
BMD	Bone Mineral Density
BSA	Body Surface Area
B.Wt	Body Weight
CCL11	C-C Motif Chemokine Ligand 11 (Eotaxin)
CXCL1	C-X-C Motif Chemokine Ligand 1 (KC)
CXCL10	C-X-C Motif Chemokine Ligand 10 (IP-10)
CRF	Corticotropin-Releasing Factor
CTX-II	C-telopeptide of Type II Collagen
DFC	Dorsal Fetlock Joint Capsule
DMEM/F12	Dulbecco's Modified Eagle Medium: Nutrient Mixture F-12
DMM	Destabilization of the Medial Meniscus
DMSO	Dimethyl Sulfoxide
EDTA	Ethylenediaminetetraacetic Acid
ELISA	Enzyme-Linked Immunosorbent Assay
G-CSF	Granulocyte-Colony Stimulating Factor
GM-CSF	Granulocyte-Macrophage Colony Stimulating Factor
GH	Growth Hormone
H&E	Hematoxylin and Eosin
HPA	Hypothalamic-Pituitary-Adrenal
IFNγ	Interferon Gamma
IL-1α	Interleukin 1-Alpha
IL-1β	Interleukin 1-Beta
IL-2	Interleukin 2
IL-3	Interleukin 3
IL-4	Interleukin 4

IL-5	Interleukin 5
IL-6	Interleukin 6
IL-7	Interleukin 7
IL-9	Interleukin 9
IL-10	Interleukin 10
IL-12	Interleukin 12
IL-13	Interleukin 13
IL-15	Interleukin 15
IL-17	Interleukin 17
IMDM	Iscove's Modified Dulbecco's Medium
IP-10	Interferon Gamma-Inducible Protein 10 (CXCL10)
KC	Keratinocyte Chemoattractant (CXCL1)
LIF	Leukemia Inhibitory Factor
LIX	Lipopolysaccharide-Induced C-X-C Chemokine
LSES	Low Socioeconomic Status
μCT	Micro-Computed Tomography
MCP-1	Monocyte Chemoattractant Protein 1
M-CSF	Monocyte-Colony Stimulating Factor
MIG	Monokine Induced by Interferon Gamma
MIP-1α	Macrophage Inflammatory Protein 1-Alpha
MIP-1β	Macrophage Inflammatory Protein 1-Beta
MIP-2	Macrophage Inflammatory Protein 2
NBF	Neutral-Buffered Formalin
NOMPC	No Mechanoreceptor Potential C
OA	Osteoarthritis
OCT	Optimal Cutting Temperature
PBS	Phosphate-Buffered Saline
Pen/Strep/Fungizone	Penicillin/Streptomycin/Amphotericin B
PFC	Palmar Fetlock Joint Capsule
PTOA	Post-Traumatic Osteoarthritis
RANTES	Regulated Upon Activation Normal T-Cell Expressed and Secreted

ROC	Relative Object Count
ROI	Region of Interest
SD	Social Defeat
Sp.	Species
SOFG	Safranin-O/Fast Green
SR	Serum Replacement
TJA	Total Joint Arthroplasty
TJBV	Total Joint Bone Volume
TNFα	Tumor Necrosis Factor Alpha
TRP	Transient Receptor Potential
TRPA	Transient Receptor Potential – Ankyrin
TRPC	Transient Receptor Potential – Classical
TRPM	Transient Receptor Potential – Melastatin
TRPML	Transient Receptor Potential – Mucolipins
TRPN	Transient Receptor Potential – NOMPC
TRPP	Transient Receptor Potential – Polycystins
TRPV	Transient Receptor Potential – Vanilloid
UCreat:SCreat	Urine Creatinine to Serum Creatinine Ratio
US	United States of America
VEGF	Vascular Endothelial Growth Factor

ABSTRACT

Osteoarthritis (OA) is a leading cause of disability globally, with higher incidence in older people and lower socioeconomic status populations. The challenges health care systems face with management of the disease highlights the importance of OA research. Many studies examine possible risk factors of knee and hip OA including obesity, smoking, and alcohol consumption. Findings support that while obesity increases risk of knee OA, smoking is not a major risk factor. These extrinsic factors are, however, associated with lower socioeconomic status, and also with anxiety and depression disorders. Up to 30% of patients with chronic knee OA have described psychological stress and decreased quality of life due to debilitating pain, but the effects of psychological stress on development of knee OA has not been described.

At the cellular level, mechanosensitive cation channels in cartilage and bone, are involved with OA, but studies looking specifically at synovium and joint capsule are limited. Transient receptor potential (TRP) channels are upregulated in joint capsule in end-stage primary shoulder OA. We were unable to identify any previous studies evaluating Piezo channel expression in musculoskeletal soft tissues, but Piezo channel antagonism reduces chondrocyte death after mechanical injury. These findings suggest channels may help regulate joint responses to repetitive loading during training or work while also contributing to protective mechanisms within the musculoskeletal system. The overall objective of this research was to investigate factors that impact OA development or the disease phenotype. Two studies evaluated the following aims: 1) demonstrate the influence of chronic psychological stress on knee OA and overall systemic health, and 2) characterize the role of mechanosensitive channels in the joint capsule in OA. The first study used a mouse chronic social defeat model paired with destabilization of the medial meniscus (DMM) surgery to create a social stress scenario during OA development. We hypothesized chronic social defeat would exacerbate knee OA structural changes and systemic inflammation. The second study aimed to explore the role of mechanosensitive channels in joint capsule during OA development in the equine. Immunohistochemistry was performed on forelimb fetlock joint capsule from horses with varying degrees of lameness to first identify TRP and Piezo channel expression. Next, fibroblasts were isolated from the tissue to determine channel activity. We hypothesized that TRP and Piezo channels are required for normal homeostasis, but are

dysregulated in OA and dysregulation contributes to fibrosis of the joint capsule. Joint capsule fibrosis leads to joint stiffening and reduced range of motion, two of the cardinal signs of OA.

The results of the first study showed OA was induced to a similar extent in both groups of mice that underwent DMM surgery. While anxiety- and depressive-like behaviors were exhibited by mice that underwent chronic social defeat episodes, unexpectedly, the majority of systemic inflammatory markers were not worse in mice with DMM and chronic social defeat compared to DMM alone. We were also able to show TRP and Piezo channel expression in one normal dorsal and palmar fetlock joint capsule sample, however, COVID-19 prevented further investigation. With our results we were able to conclude that while chronic social stress influences development of OA, in the current experiments, neither systemic inflammation nor structural signs of knee OA were worse with chronic social stress. We hope that exploration of OA through these two studies will help us understand how the disease contributes to overall systemic dysfunction while also providing a baseline for future development of TRP and Piezo channel modulators to prevent joint pathologies.

CHAPTER 1. INTRODUCTION

Osteoarthritis (OA) impacts human quality of life worldwide as the most common musculoskeletal disorder. The age range at diagnosis is between 24 and 74 despite peak incidence occurring in people aged 55 to 64 years (Bortoluzzi, Furini, & Scire, 2018; Guilak, 2011; O'Neill, McCabe, & McBeth, 2018). Epidemiologic studies in elderly individuals (>70 years of age) show that as age increases, there is higher OA prevalence in female individuals (Felson et al., 1987; O'Neill et al., 2018). Other risk factors that have been identified are commonly related to joint conformation and biomechanics, genetics, metabolism, obesity, diet, and lifestyle. Studies have also shown that populations determined by low socioeconomic status (LSES) have a higher risk (Korda, Paige, Yiengprugsawan, Latz, & Friel, 2014; Vina & Kwoh, 2018).

The economic burden of OA is substantial. As an example, many patients with OA undergo total joint arthroplasty (TJA) for end-stage disease to preserve function and reduce pain. TJA contributes substantially to the direct costs associated with OA. In the USA alone in 2009, the estimate for the cost of TJA was $42 billion. Total hip arthroplasty cost, specifically, ranged from $11,000 to $126,000 per patient depending on location, length of stay, and post-operative rehabilitation (Hiligsmann et al., 2013). Although there are many factors influencing the cost of the disease, disability causing loss-of-work can be considered an indirect cost and is often considered in economic studies of the disease. One study from Canada reported that OA was the reason for 44.4% of individuals claiming unemployment due to illness (Bortoluzzi et al., 2018). Impacts of chronic disease expand beyond financial and physical burden, however. Psychologic health is impacted as well. People with chronic disease have a higher prevalence of depression and anxiety disorders (Korda et al., 2014). These burdens will continue to impact all populations as life expectancy increases over time (Bortoluzzi et al., 2018).

Pathologically, OA is characterized by loss of articular cartilage, and is considered a whole joint disease, involving pathology of bone, synovium, joint capsule, menisci, and ligaments (O'Neill et al., 2018). A normal synovial joint functions to create near-frictionless motion with normal physiologic loading. Development of articular cartilage structure is influenced during post-natal growth, but ultimately becomes highly organized with three different zones of cartilage covering subchondral bone. The superficial layer of chondrocytes are elongated and oriented parallel to the joint surface. These cells contribute to frictionless movement by producing

hyaluronate, phospholipids, and lubricin. The other zones, transitional zone and deep zone, are areas of large, round chondrocytes. Transitional zone chondrocytes are randomly organized while deep zone chondrocytes are stacked perpendicular to the articular cartilage surface. Highly organized collagen II fibrils comprise 90% of the extracellular matrix and contribute to the joints' biomechanical properties (Caron, 2003; Decker, 2017). Aggrecan is the most abundant proteoglycan within the extracellular matrix, and it forms aggregates with hyaluronan. Articular cartilage receives its nutrients from the synovial joint capsule. The joint capsule structure encloses the synovial space where denser connective tissue is found in areas more at risk of injury. The interior joint capsule is covered by the synovial lining, or synovial intima, that is comprised of synoviocytes. These cells are typically divided into three main types: macrophage-like, fibroblast-like, or an intermediate cell form with characteristics of both (Wilkinson, Pitsillides, Worrall, & Edwards, 1992). Type B synoviocytes, or the fibroblast-like cells, are the primary cell type within the tissue, accounting for 80-90% of the cells. The other 10-20% of cells are phagocytic in nature (Caron, 2003; Wilkinson et al., 1992). The subsynovial region lies under the synovial lining and is responsible for producing synovial fluid and exchanging metabolic wastes and nutrients (Caron, 2003).

Under normal physiologic conditions each joint can withstand loads up to 10 times the body weight. During this loading, chondrocytes maintain cartilage microarchitecture homeostasis. Normal turnover within the cartilage is a function of chondrocyte response to both underlying genetic and environmental cues from the extracellular matrix. Breakdown of normal cartilage occurs if there is an interruption in this metabolic balance (Guilak, 2011). Chondrocytes as a whole, however, have poor reparative capabilities. Once the frictionless motion of the joint is disrupted, a vicious cycle occurs worsening the condition over time (Decker, 2017). Although the disease is largely characterized as primary, where no definitive etiology can be determined, it has been estimated that up to 10% of OA cases in America are considered secondary OA (Furman et al., 2007; O'Neill et al., 2018). Secondary causes of OA most commonly include subchondral bone fracture or articular cartilage fracture, but could encompass any traumatic injury involving the soft tissue of the joint (Furman et al., 2007).

The most common joints affected by OA in humans include hip, knee, and hand, but any joint may be affected (O'Neill et al., 2018). Most patients report pain, stiffness, and loss of function in the joint before diagnosis. Radiographic evidence is required for a definitive diagnosis, and may

include joint space narrowing, osteophyte development, and subchondral bone sclerosis. These features are typically combined into a scoring system for recording disease severity. There is not always a correlation between radiographic evidence of the disease and clinical picture, however. Radiographic evidence of OA can be present in up to 50% of asymptomatic patients. Additionally, some people remain relatively stable for long periods of time, while others progress quickly to debilitating pain (Hiligsmann et al., 2013; O'Neill et al., 2018).

Limited understanding in the progression of the disease has impacted the range of treatments available. The most severe, end stage cases may be eligible for TJA, but treatment at earlier time points is largely palliative in nature. For example, non-steroidal anti-inflammatory drugs are typically given to decrease inflammation and pain in the joint to facilitate continued mobility. Several life-style modifications, where appropriate and applicable, can reduce disability (Guilak, 2011; Hiligsmann et al., 2013). The challenges faced by the general public and health care systems with management of the disease, cost of treatment, and overall impact on quality of life highlight the importance of OA research.

1.1 Specific Aims

OA research can be divided into multiple focuses. Epidemiological, clinical, and bioengineering are among the most popular topics, but gaps still exist among and between concentrations. In order to bridge these gaps, the goal of this thesis was to investigate extrinsic and intrinsic factors that impact OA development or the disease phenotype. Two studies were established to achieve the following aims: 1) demonstrate the influence of chronic psychological stress on knee OA and overall systemic health, and 2) characterize the role of mechanosensitive channels in the joint capsule in OA.

To address the first aim, the study utilized a mouse chronic social defeat model paired with DMM surgery to simulate social stress scenarios during post-traumatic OA (PTOA) development. The **global hypothesis** of this aim was chronic social defeat would exacerbate knee OA structural changes and systemic inflammation. Experiments were designed to observe responses in classical biomarkers and cytokines involved in OA and stress, identify gastrointestinal inflammation as a connection between systemic health and chronic stress, and determine the severity of OA developed across experimental groups.

The second study was developed to explore intrinsic factors that may lead to joint stiffening or loss of range-of-motion, as cardinal signs of OA. Specifically, we wanted to identify the role of mechanosensitive channels in joint capsule tissue in equine fetlock OA. Equine tissues were used because the species commonly experiences high intensity training as a part of their day-to-day life, and tissues from a wide range of disease states (normal – end-stage) are frequently available from cadavers, in contrast to the availability of human tissues. The stride patterns of the equine limb could be considered for modeling repetitive mechanical loading, similar to repeated manual labor for shoulder OA in humans. Use of immunohistochemistry allowed us to first identify the expression of mechanosensitive channels within joint capsule tissue from horses, since this has not been previously done. We also isolated fibroblasts from fetlock joint capsule to determine transient receptor potential channel (TRP) and Piezo channel activity. We expected that specific isoforms of TRP and Piezo channels involved would be identified through the modulation of cells' ability to cause contraction of a collagen gel under the influence of various TRP and Piezo channel agonists or antagonists. We hypothesized that mechanosensitive channels are required for both normal homeostasis and tissue adaptation to training. Ultimately, we believe repetitive mechanical loading could cause dysregulation in expression during supra-physiologic loads, contributing to fibrosis of the joint capsule and OA.

Exploration of OA through these two studies will help us understand overall systemic health in relation to OA. Not only will we gain perspective on the disease itself, but how chronic stress may impact the condition. We also hope that the equine study will provide a baseline for developing channel modulators fortargeting joint pathologies. Ultimately, we hope both studies will provide a better understanding of OA progression in humans, and potentially assist with future prevention of the disease.

CHAPTER 2. LITERATURE SEARCH

2.1 Chronic Social Stress and Osteoarthritis

OA is a heterogeneous disease that presents differently in each individual (Bortoluzzi et al., 2018). Risk factors range from lifestyle choices, such as alcohol consumption, to non-modifiable factors, such as genetics (O'Neill et al., 2018). Studies have shown lifetime risk of symptomatic OA is as high as 40% depending on gender and obesity. Prevalence of OA is disproportionately higher in LSES populations. Up to 50% of people in these populations have an increased risk of knee OA. One cause for heightened risk in LSES areas is due to the population also having increased prevalence of OA risk factors, namely obesity. Knee OA risk decreased by 25% in LSES populations when corrected for obesity, but a 25% higher risk is still obviously skewed compared to a 14% risk in the US general population (Bortoluzzi et al., 2018; Reyes et al., 2015).

The impact of OA is present worldwide, and there is a need for a better understanding of the disease as life expectancy rises (Reyes et al., 2015). In more severe cases, the cost of end-stage disease treatment may be prohibitive in LSES areas that do not have easily accessible health care. LSES individuals are more likely to cope with pain in order to continue working (Vavken & Dorotka, 2011). Therefore, there is an urgent need to mitigate the prevalence of OA, its progression, and the impact of OA on both individuals and communities. Burdens are not limited to pain and finances in many cases, however. The impact of coping with chronic pain leads to anxiety and depression. Up to 30% of patients with knee OA describe psychological distress. Moreover, LSES populations have an increased prevalence of depression and anxiety (Olvera Alvarez, Kubzansky, Campen, & Slavich, 2018). Psychologic stress has been linked to worsened pain, but highly depends on the person's level of perceived pain. Factors influencing perceived pain may depend on how the pain impacts an individual's day-to-day life. For instance, weight bearing pain and non-weight bearing pain may impact individuals differently based on their occupation (Iijima et al., 2018). Furthermore, some studies have correlated depression to poorer outcomes post-operatively, and lower motivation to return to normal function (Khatib, Jenkin, Naylor, & Harris, 2016).

The major limitation in the studies described above is the subjectivity of perceived pain. This is especially apparent in studies looking to find correlation between clinical signs and

development of OA. The vast majority of clinical-based studies highlight the fact that OA radiographic diagnosis does not determine the severity of the disease (Hiligsmann et al., 2013). Although many risk factors are appreciated, OA is a multi-factorial disease (Guilak, 2011). This highlights the importance of expanding OA research to include both functional and biologic outcome measures. Clinical studies involving OA are largely focused on risk factors, predictive values, and progression of the disease, but they fail to create an understanding of how OA and comorbidities interact and influence systemic health. One study from Canada reported that 52.1% of patients with OA also had four or more other medical conditions. Back problems, high blood pressure, and allergies were overrepresented. Furthermore, all OA patients reported at least one other medical condition even though mental health related conditions were not reported in this study. Instead, the comorbidity data was correlated with sociodemographic information and health-related quality of life measures (Tarride et al., 2012). To the best of our knowledge, the impact of psychosocial stress on OA development has not been explored.

Stress models are widely used in animal studies to measure the effects of depression on health conditions (Toyoda, 2017). They are also commonly used to test anti-depression and anti-anxiety medications. The validity of testing anti-depression medications with some stress-induced animal models is questionable, however. The forced swim and tail suspension tests are acute stressors. Therefore, medications tested under these conditions show promising results, but fail to show benefit in clinical trials. In contrast, human depression disorders require long term use of medication before results are seen (Cryan & Holmes, 2005). As chronic social defeat models were developed, medication testing became more accurate. The development of chronic social defeat models has improved our ability to look at long term effects of depression in a wide range of studies. Chronic social defeat models have been tested in many species including mice, rats, pigs, zebra fish, and crickets. Mice are among the most popular models (Toyoda, 2017). Specifically, the resident-intruder model has been used widely in both rats and mice. When performed with mice, this model most commonly utilizes naturally aggressive CD-1 male mice for the resident and C57BL/6J male mice as the intruder. Swiss Webster mice may also be naturally aggressive and used as resident mice (Newman et al., 2019). On the other hand, other intruder mice commonly used are BalbC or 129SvEv strains (Dadomo et al., 2011; Razzoli, Carboni, Andreoli, Ballottari, & Arban, 2011). Appropriate screening is required for aggressive mice. Aggressiveness is often measured by attack latency and attack bite frequency (Newman et al., 2019). Continued

stress is provided between the defeat episodes, where each singly housed mouse is housed within a cage containing a transparent divider between the "resident" and the "intruder" sides. The divider allows for visual, olfactory and auditory interaction, but no physical altercation while prolonging stress periods. During social defeat sessions, the "intruder mouse" is introduced to the "resident" mouse side of the cage. Sessions last five to ten minutes for ten consecutive days. Intruder mice should be rotated through several CD-1 partners to prevent acclimation. One of the benefits of this particular chronic social defeat protocol is the adaptability to individual studies. Additional sessions may be introduced as the experimenter wishes to observe different outcome measures (Golden, Covington, Berton, & Russo, 2011). For instance, the initial episodes that occur once per day for ten consecutive days are known to show immediate increases in heart rate, ACTH, and corticosterone. Avoidance behavior and polyphagia are also noted alongside these episodes. If additional episodes are introduced regularly (e.g. every other day or every 72 hours) over the course of longer periods of time, rats and mice also exhibit immobility, anhedonia, and weight loss (Hollis & Kabbaj, 2014).

Anxiety- and depression-like behavior outcome measures in chronic social defeat models are commonly identified via behavioral analysis. If the mice are singly housed, behaviors that are observed in chronic social defeat models can be as simple as eating habits or drinking frequency. The C57BL/6J mice often increase eating and become polydipsic (Hollis & Kabbaj, 2014). Weight gain can be associated with polyphagia as an anxiety-like response, however, there are conflicting reports about the influence of chronic social defeat on weight. Some studies show weight gain and others show weight loss. Both the Goto et al and Krishnan et al studies initially used the resident-intruder model as previously described with C57BL/6 and CD-1 mice. Due to the severity of injuries, the amount of time mice were subjected to chronic social defeat episodes was decreased from 5 minutes after the first interaction to 0.5 minutes after the first interaction in the Goto et al. study. These mice exhibited weight gain throughout the course of both stress periods and recovery periods. Mice in the Krishnan, et al study, however, exhibit weight loss after their ten days single of chronic social defeat episodes with no recovery period. (Goto et al., 2014; Krishnan et al., 2007). Loss of sucrose preference (a test of anhedonia) is also demonstrated in studies. Other tests to evaluate anxiety- and depressive-like behaviors, outlined in the review by Cryan & Holmes, include observing specific avoidance behaviors and immobility behaviors. Two examples of tests that can be used for these are light-dark emergence tests and tail-suspension tests, respectively.

The light-dark emergence test expects anxiety driven mice to increase their latency to emerge from the dark. In other words, they avoid well-lit areas. Tail suspension tests measure how long it takes for the mouse to exhibit passive immobility while being hung by their tail. Typically, more depressed mice stay immobile for longer compared to control mice (Cryan & Holmes, 2005; Toyoda, 2017).

Although there is a wide range of behavioral tests that can support evaluation of anxiety- and depression-like behaviors, biologic factors are also evaluated in neurobehavioral studies. Certain biomarkers can be viewed directly as measures of stress or related pathways. Corticosterone, corticotropin-releasing factor (CRF), and brain-derived neurotrophic factor (BDNF) are examples of markers for anxiety- or depression-like disorders (Mallei, Ieraci, & Popoli, 2019; McQuaid, Audet, Jacobson-Pick, & Anisman, 2013; Niraula, Wang, Godbout, & Sheridan, 2018). Corticosterone is the rodent analog of human cortisol. Regulation of corticosterone levels are driven by the hypothalamic-pituitary-adrenal (HPA) axis (Raubenheimer, Young, Andrew, & Seckl, 2006). As a response to stress, the HPA axis releases CRF and downstream glucocorticoids are elevated (Smith & Vale, 2016). Because of this axis, CRF elevation may also be observed in anxiety or depression disorders (McQuaid et al., 2013). BDNF, as a neurotrophic factor, is responsible for survival and protection of neurons within the nervous system. It has been studied extensively in anxiety, depression, and neurodegenerative diseases. Previous studies show that decreased brain tissue BDNF is associated with anxiety and depression (Bathina & Das, 2015). Also, it is well known that depression and inflammatory conditions are closely associated. Some studies have evaluated inflammatory markers, or inflammatory cell populations, along-side neurobehavioral pathways (Stewart et al., 2015; Toyoda, 2017).There is increasing evidence that leukocytes and their inflammatory effector molecules may be related to chronic social defeat through β-adrenergic signaling (Powell et al., 2013).

Animal PTOA models are also widely used throughout orthopaedic research. Each model varies based on species, joint, target within the joint, and mechanism of disease induction. Knee OA, specifically, can be induced in several different ways: Controlled exterior impact of the medial femoral condyle in rabbits is one example. Surgical disruption may also be done by destabilizing the joint through transection of supportive tissues, such as the cruciate ligaments or menisci (Martin et al., 2017). DMM is a popular surgical model of knee joint PTOA. The surgery involves transecting the medial meniscotibial ligament. In the past, these surgeries have been done on larger

animals because of the technical challenge mice pose, but the method was described in mice thirteen years ago. Histologic evidence of OA is evident within two weeks, in contrast to the spontaneous model of mouse OA which may take up to two years to develop (Glasson, Blanchet, & Morris, 2007).

Outcome measures for research models of OA range from direct pain testing of the animals to microscopic evaluation of the joint after euthanasia. Pain-related outcome measures of OA may involve gait analysis or reflexive pain measures. Gait analysis observes the animal's locomotion and different force plates may be used to measure changes. The reflexive pain measures typically test responses to noxious stimuli with the goal of identifying hyperalgesia or analgesia. Hot plate tests and tail flick tests involve applying heat to either the paw or tail, respectively. The amount of time the mouse takes to move or lick the area is measured. If the animal is hyperalgesic, it will attempt to remove the stimulus faster than a non-painful animal, conversely, analgesia, or reduced responsiveness is also observed (Gregory et al., 2013).

Imaging of the whole animal or individual joints is also possible. Micro-computed tomography (μCT) is a popular modality for imaging bones because of the detail 3D images can provide on such a small scale. Several measures of bone characteristics can be gathered from the scans, including bone mineral density (BMD), total joint bone volume (TJBV), and trabecular thickness (Carballo et al., 2018). BMD and trabecular thickness each give indications of the strength of the bone and its capability of withstanding forces. Higher BMD and increased trabecular thickness are typically associated with worse OA because of their connection to bone remodeling (Cai et al., 2020; H. L. Stewart & Kawcak, 2018). TJBV is also an indicator of OA because of osteophyte development (O'Neill et al., 2018).

An additional way of analyzing OA severity is through histologic analysis. Safranin-O/Fast Green (SOFG) staining is the most common way of analyzing joint articular cartilage. With SOFG, the proteoglycan within the cartilage is stained red with Safranin-O, and collagens are stained green with Fast Green. Modified Mankin scoring allows evaluation of seven cartilage characteristics where increasing scores indicate worse OA. The categories of the Modified Mankin score include: articular cartilage structure, tidemark duplication, loss of safranin-O staining, fibrocartilage development, chondrocyte clones present in the un-calcified cartilage, hypertrophic chondrocytes in the calcified cartilage, and subchondral bone thickness. Knee OA analysis usually scores based on quadrants (medial femur, medial tibia, lateral tibia, and lateral femur), and each

quadrant scores from 0-30 points (Furman et al., 2007). Quadrant scores are summed to generate a total joint score. An additional scoring system, the Modified Krenn system does not look at OA directly. Instead, the six-point scoring system addresses the degree of synovitis associated with each joint quadrant (Lewis et al., 2011).

As with psychologic testing, inflammatory markers and other biomarkers may be measured from different tissues. C-telopeptide of type II collagen (CTX-II) is released as a degradation product as cartilage breakdown progresses (Duclos et al., 2010). Interleukins and chemokines are also measured frequently as indicators of inflammation, and most studies look at multiple markers. They are commonly measured from synovial fluid, but they may also be isolated from serum or plasma (Haraden, Huebner, Hsueh, Li, & Kraus, 2019).

2.2 Equine Fetlock Osteoarthritis

Musculoskeletal disease in equine patients is one of the leading reasons for euthanasia after gastrointestinal disease and reproductive disease. According to owners, lameness is an important indicator of quality of life. Geriatric horses are less likely to have musculoskeletal issues secondary to a traumatic event than younger individuals, but chronic musculoskeletal conditions are frequently taken into account in assessing quality of life before euthanasia (McGowan & Ireland, 2016). Additionally, lameness is the most common cause of a racehorse losing training days (Reed et al., 2012). Galloping racehorses have a natural four-beat gait that results in complete weight bearing on a single limb, namely the leading forelimb. The metacarpophalangeal (fetlock) joint of this limb is at the highest risk of injury because of the degree of flexibility in the joint and the amount of counter support musculoskeletal tissues in this area are required to provide (Richardson & Dyson, 2011). Studies show the dorsal-flexion angle of the leading forelimb's fetlock joint can decrease as many as 30 degrees during maximum speeds (Butcher & Ashley-Ross, 2002). This significantly increases the tension on the palmar fetlock joint capsule (PFC), as well as the tendons and ligaments that span the palmar aspect of the joint. Compression of the dorsal fetlock joint capsule (DFC) may also occur as the third metacarpal bone and proximal phalanx impinge upon one another. During training and racing, the repetitive nature of these forces contributes to the number of injuries and poor performance complaints seen in clinics (Butcher & Ashley-Ross, 2002; Richardson & Dyson, 2011).

Thoroughbred racehorses that undergo vigorous training are at risk of many different types of injuries, including catastrophic and overuse injuries. The top three most common causes of lameness are due to injuries to the foot, fetlock joint, or suspensory ligament. Causes for lameness in the fetlock joint can be further divided into synovitis, metacarpal bone III diseases, fractures, or OA. Fetlock OA in horses has been widely accepted as a multi-factorial disease, similar to humans. The most common hypothesis for OA development in horses involves healthy cartilage being damaged by extreme mechanical forces. Repetitive mechanical loading, as we also see in human athletes, causes micro-trauma to the articular cartilage and worsens with time (Caron, 2003). Chronic synovitis leading to OA typically occurs due to overuse injury. The most common clinical signs of synovitis include heat, effusion, pain, and mild lameness (Richardson & Dyson, 2011).

Identification of OA may be done with arthroscopic examination after lameness exam and other diagnostic imaging is completed. Treatments are not curative since the articular cartilage cannot be repaired, but fractures can be repaired and osteochondral fragments removed. Otherwise, the condition will only worsen. One challenge that occurs specifically with treatment of OA in racehorses is the expectation for performing despite having a debilitating, chronic condition. Studies show that overuse of intraarticular corticosteroids exacerbates the disease, but more studies need to be done to see if this is directly due to treatment or due to continued use of the joint. Other treatments for OA include intra-articular hyaluronan, systemic or intra-articular anti-inflammatories, rest, and rehabilitation (Arthur, Blea, Ross, Moloney, & Cheney, 2011; Butcher & Ashley-Ross, 2002). Up to 60-80% of joint capsule injuries seen will reoccur (Richardson & Dyson, 2011). Ultimately, if poor performance continues or the injury reoccurs, the racehorse will be retired (Arthur et al., 2011).

As described in the introduction chapter, progression of OA is largely caused by the poor reparative properties in both joint capsule and articular cartilage. Mature chondrocytes and synoviocytes have slower turnover compared to other tissues, and the structure of mature joint tissue is highly organized. After injury, these tissues have a general loss of cell-cell communication as white blood cells infiltrate the area and contribute to break down of the extracellular matrix. These conditions begin a vicious cycle of cartilage break down and synovial fibrosis (Decker, 2017). Idiopathic cases of OA raise many questions about how, and when, normal cellular communication changes to have deleterious effects.

Translation of biomechanical loading to cell signaling occurs through mechanosensitive cation channels, such as those found in TRP channel, Piezo channel, and acid-sensing ion channel (ASIC) families. All three channel families are known for their roles in translating mechanical load to an electrochemical gradient. TRP, Piezo, and ASIC channels are permeable to cations, but TRP and Piezo are most notably permeable to calcium, and ASICs are more permeable to sodium (Coste et al., 2010; Cristofori-Armstrong & Rash, 2017; Zheng, 2013). ASICs, however, are better known for their gating mechanism by protons associated with acidosis, ischemia and inflammation (Cristofori-Armstrong & Rash, 2017; Pignataro et al., 2011). Although ASICs are not the primary focus of the present study, research increasingly incorporates their observation alongside other mechanosensitive channels due to their commonalities in responses to inflammatory pathways (Holzer, 2015; Kobayashi, Yoshiyama, Zakoji, Takeda, & Araki, 2009).

The TRP channel family is divided into seven subfamilies based on sharing structure and sequence: TRPN, TRPC, TRPM, TRPV, TRPA, TRPP, and TRPML. Each subfamily is expressed in mammals, except TRPN. TRPML and TRPP are unique in their discovery, and naming. They are primarily involved with genetic mutations that cause disease and least resemble the remaining channels (*Neurobiology of TRP Channels*, 2017). The TRPC family most resembles the original channel found in blind *Drosophila* sp. in 1969. They are most well known for their involvement in sight (Minke, 2010). TRPM is the most diverse channel, where "M" stands for melastatin. They are unique in their structure because three out of four channel members have an enzymatic domain within their protein (Hantute-Ghesquier, Haustrate, Prevarskaya, & Lehen'kyi, 2018). TRPV and TRPA, the main focus of this thesis, have their own unique qualities and will be described in detail below.

TRPA is a small subfamily with only one channel identified thus far, TRPA1. This channel is unique because it has the longest Ankyrin repeat of those found with similar structure. This channel is highly conserved across all species spanning insects to mammals. Although TRPA1 channels have been primarily discovered in sensory neurons, recent findings have described them in joint capsule tissue, cardiomyocytes, human embryonic kidney cells (HEK293T), and lung cells (Andrei et al., 2017; Buch, Buch, Boekhoff, Steinritz, & Aigner, 2018; Chainani et al., 2020; Viana, 2016; Wang et al., 2018). Mechanical and thermal sensation mediated by this channel has been studied in mammals, and TRPA1 has become known as the "noxious cold sensor." Chemical stimulation has also been studied. The range of chemicals, and oxidative stress products, TRPA1

can respond to include mustard oil, cinnamaldehyde, and allicin. Cinnamaldehyde is an example of an agonist specific to TRPA1 (*Neurobiology of TRP Channels*, 2017). TRPA1 can also sense inflammation and tissue damage through reactive oxygen species (Viana, 2016). Trigeminal neurons, dorsal root ganglion neurons, and nodose neurons possessing this channel play a role in detecting noxious stimuli alongside the vanilloid type 1 TRP channel (TRPV1) (Andrei et al., 2017). Research about TRPA1 involvement in the musculoskeletal system mostly focuses on skeletal muscle sensory neurons. One study, however, has identified the channel in human primary OA chondrocytes (Nummenmaa et al., 2016).

The TRPV family includes six channels named because TRPV1 responds to the vanilloid, capsaicin. Of these six channels, TRPV1 and TRPV4 are most relevant to this study due to their involvement in pain sensation and inflammation (*Neurobiology of TRP Channels*, 2017). TRPV1 has been identified within sensory neurons, vascular smooth muscle cells, and endothelial cells. It can be activated by noxious heat, capsaicin, and protons. Inflammatory mediators and neurotransmitters have also been found to sensitize the channel to calcium ions (Zhao & Tsang, 2017). Similarly, TRPV4 has been found in sensory neurons, and plays a role in several different types of pain (*Neurobiology of TRP Channels*, 2017). TRPV4 also has a wide range of activators including, but not limited to, mechanical activation, inflammatory mediators, and UV light (*Neurobiology of TRP Channels*, 2017). Table 1 below summarizes the types of pain TRP channels are involved in, as adapted from *Neurobiology of TRP Channels*, 2nd Edition.

Table 1. TRP Channel Involvement in Pain

TRPA1	**TRPV1**	**TRPV4**
Nociceptive	Neuropathic	Neuropathic
Inflammatory	Inflammatory	Inflammatory
Pain Syndromes	Visceral	Visceral
		Trigeminal

As with TRPA1, research involving TRPV1 and TRPV4 largely focuses on their roles in neurobiology. While musculoskeletal research with these two channels has been limited mainly to

cartilage and muscle, both have been identified. TRPV1 has been identified in sarcoplasmic reticulum of mouse skeletal muscle (Lotteau, Ducreux, Romestaing, Legrand, & Van Coppenolle, 2013). TRPV4 research shows activation of the channel can improve mechanical properties of articular cartilage constructs (Eleswarapu & Athanasiou, 2013). TRPV4 plays a role in regulating chondrocyte matrix metabolism (O'Conor, Leddy, Benefield, Liedtke, & Guilak, 2014). The same group that performed the preceding study, also found that TRPV4 knock out mice have decreased incidence of age-related OA in adults (O'Conor et al., 2016).

Piezo channels, while a newer discovery, are also mechanically activated proteins (Ge et al., 2015; Volkers, Mechioukhi, & Coste, 2015). Mammals have two members of this channel family: Piezo1 and Piezo2. Although both channels are considered mechanosensitive, their tissue distribution is slightly different. Piezo2 responds to mechanical stimulation through sensory tissue while Piezo1 is found more commonly in non-sensory tissues (Coste et al., 2010; Wu, Lewis, & Grandl, 2017). Specifically, Piezo1 is important in organs subjected to constant stretch and shear forces. This includes gastrointestinal enterochromaffin cells, vascular cells, and tenocytes (Alcaino, Farrugia, & Beyder, 2017; Hyman, Tumova, & Beech, 2017; Passini et al., 2019). Lee, et al studied the characterization of both Piezo1 and Piezo2 in chondrocytes. The study showed that both channels synergistically contribute to chondrocyte mechanosensitivity, and inhibition of these channels protects chondrocytes from mechanical injury (Lee, Guilak, & Liedtke, 2017; Lee et al., 2014).

To date, musculoskeletal studies involving either TRP or Piezo channels are predominantly focused on tendon, muscle, or cartilage, as explained above (Gavenis et al., 2009; Lee et al., 2014; Lotteau et al., 2013; O'Conor et al., 2014; O'Conor et al., 2016). Only one study has been performed to identify TRP channels in human joint capsule tissue. TRPA1, TRPV1, and TRPV4 were identified in the anterior shoulder joint capsule of patients that underwent total shoulder arthroplasty for primary OA treatment. The channels were localized to the area of the capsule that experiences supra-physiologic levels of stretch during overhead manual labor or activities (Chainani et al., 2020). Other studies related to joint capsule focus on synoviocytes. One study identified TRPV4 in OA synoviocyte progenitor cells and normal cells, with differential expression across groups (Bertram, Banderali, Tailor, & Krawetz, 2016). The Muraki group in Japan similarly found TRPV4 mRNA expression in human synoviocytes (Itoh et al., 2009).

The topic of mechanosensitive channels has become increasingly popular in the last decade, however, their role in musculoskeletal disease is still a developing research topic. Many studies discuss the clinical role of biomechanics in OA, but few studies translate this discussion to the propagating factors as an imbalance of homeostasis. The results of the Chainani, et al study provide premise to exploring mechanosensitive channels in equine patients because the fetlock joint is naturally subjected to repetitive mechanical loading similar to human subjects who perform repeated overhead activity as part of manual occupations.

CHAPTER 3. CHRONIC SOCIAL STRESS AND OSTEOARTHRITIS

3.1 Chronic Social Stress and Osteoarthritis Methods

3.1.1 *Animals, Surgery, & Tissue Collection*

As a part of a larger study, the animal procurement, surgery protocols, neurobehavioral testing, and tissue collection occurred at Duke University following IACUC approval. Twelve-week old male, C57BL6/J mice (The Jackson Laboratory, Bar Harbor, ME, USA) were purchased and allowed to acclimate for two weeks, single housed. Each animal was randomly assigned to one of three experimental groups: Sham (n=10), Destabilization of the Medial Meniscus (DMM) (n=14), or DMM with Chronic Social Defeat Stress (DMM+SD) (n=14). A resident-intruder model was used as described in Golden, et al, to induce chronic social stress in DMM+SD mice beginning at 14-weeks of age (Golden et al., 2011). Aggressive retired male breeder CD-1 mice were used during once daily social defeat episodes for ten days. At 16-weeks of age, all mice underwent surgery. Mice in the Sham group, underwent a sham surgery to visualize the medial meniscotibial ligament, and DMM was performed in the left limb of all remaining mice. The right limb was considered an unoperated control limb for the remainder of the study. After two weeks of recovery, DMM+SD mice underwent additional social defeat episodes twice per week until neurobehavioral testing at 26 weeks of age, then the mice were euthanized at 28-weeks old. One mouse in DMM+SD died prematurely and was not available for analysis.

Neurobehavioral testing included light-dark emergence test, tail suspension test, sucrose preference testing, hot plate test, tail flick test, grip strength, Von Frey testing, and gait analysis. In summary, the results of these tests showed that DMM and DMM+SD groups had significant differences consistent with increased anxiety- and depressive-like behaviors and anhedonia, but DMM+SD demonstrated these changes to a greater extent. Unexpectedly, gait analysis showed that while DMM mice were asymmetric in their hindlimb gait, DMM+SD mice were not. This was accompanied by unexpected mechanical, but not thermal, analgesia in DMM mice; whereas DMM+SD mice demonstrated relative mechanical hyperalgesia compared to DMM mice (results not shown).

The mice were also weighed prior to euthanasia. These weights, seen in Figure 1 on the next page, were used with treadmill videos from neurobehavioral data (animal length

measurements) to retroactively calculate body surface area (BSA). BSA was calculated according to the formula outlined in Rodrigues et al: $BSA = Weight\ (W)^{0.425} \times Length\ (L)^{0.725} \times 0.007184$ (Rodrigues, Miguel, Napimoga, Oliveira, & Lazo-Chica, 2014). BSA was used for calculations described later in this thesis. Samples collected at the time of euthanasia included serum, urine, sections of gastrointestinal tract, and stifle joints. Additional samples were collected, but were not used for the current study.

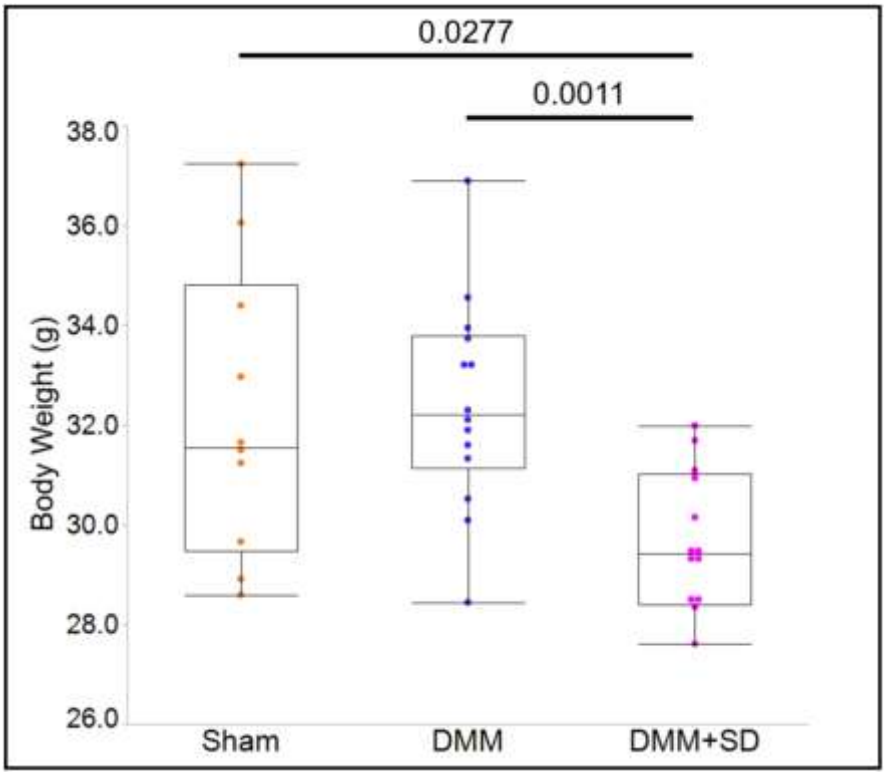

Figure 1. Body weights of mice (n=37) at euthanasia ($p<0.05$).

3.1.2 *Cytokines and Biomarkers*

Blood and urine were collected at time of euthanasia from all mice. Blood was spun down to isolate the serum. To evaluate systemic inflammation, 37 serum samples were sent to Eve Technologies Corporation (Calgary, AB, Canada) for a 31-plex cytokine analysis. The values included on the cytokine array were eotaxin (CCL11), G-CSF, GM-CSF, IFNγ, IL-1α, IL-1β, IL-2, IL-3, IL-4, IL-5, IL-6, IL-7, IL-9, IL-10, IL-12 (p40), IL-12 (p70), IL-13, IL-15, IL-17, IP-10 (CXCL10), KC (CXCL1), LIF, LIX, MCP-1, M-CSF, MIG, MIP-1α, MIP-1β, MIP-2, RANTES,

TNFα, and VEGF. All samples were diluted 1:2 in 1X Phosphate-Buffered Saline (-/-) (PBS) prior to shipment.

Thirty-one of the 37 samples for which adequate serum was available were also sent for a pituitary 3-plex analysis. The pituitary assay measured values for BDNF, Growth Hormone (GH), and Prolactin. The samples sent for the pituitary analysis were diluted by the company during the assay protocol.

Serum CTX-II, serum corticosterone, serum creatinine, urine CTX-II, urine corticosterone, and urine creatinine were also measured from all 37 mice by Enzyme-Linked Immunosorbent Assay (ELISA). Protocols for the ELISAs were followed according to manufacturer's kit recommendations (MyBioSource.com, San Diego, CA, USA). All plates were read on a Spectramax i3x microplate reader (Molecular Devices LLC, San Jose, CA, USA) at 450 nm, and standard curves were developed in the SoftMax Pro software (Molecular Devices LLC, San Jose, CA, USA).

Body weight, urine creatinine, serum creatinine, and BSA values were used to create three normalization methods that were applied to all serum values obtained. Values were normalized to body weight (B.Wt) alone, urine to serum creatinine ratio (UCreat:SCreat), and the urine to serum creatinine ratio adjusted for BSA ((UCreat:SCreat)/BSA).

3.1.3 *Gastrointestinal Histology*

Sections of jejunum, ileum and colon were collected from all 37 mice at the time of euthanasia. Samples were fixed with 10% Neutral-Buffered Formalin (NBF) and 70% ethanol prior to being processed for histologic staining. Purdue University Research Histology Laboratory prepared paraffin slides of all three sections and stained for hematoxylin and eosin (H&E) and F4/80+ macrophages. Slides were imaged using an Olympus BX53 upright microscope in conjunction with the Olympus CellSens Dimensions program (Olympus Corporation, Shinjuku City, Tokyo, Japan). For all sections, camera settings, exposure, and white balance were determined prior to imaging and collecting data to ensure each section of gut was analyzed under the same conditions. Two thresholds were also determined within the CellSens Dimensions Count & Measure add-on to differentiate between positive (F4/80+ macrophage) staining and counter-staining (nuclei).

A region of interest (ROI) was determined based on villus and crypt morphology. One ROI included one complete villus and a corresponding area of submucosa and muscularis. Three to four ROIs were selected per mouse, per section, of gastrointestinal tract based on the quality of the section. Area Fraction ROI (AF ROI) and Relative Object Count (ROC) were obtained from the Count & Measure add-on after thresholds were applied to the ROI. AF ROI corresponded to the percentage of the ROI occupied by either threshold. ROC described the percentage of one threshold compared to the other.

3.1.4 *Knee Micro-Computed Tomography (μCT)*

Paired hind limbs from all 37 mice were carefully dissected to expose the stifle joint prior to μCT imaging. Knees were stored, frozen, wrapped in saline soaked gauze at -80^{o}C prior to imaging. All knees were positioned using a 1.5mL Eppendorf tube to prevent movement during scanning. A Perkin Elmer®, Quantum GX μCT Imaging System (Perkin Elmer Inc, Waltham, MA, USA) at Purdue University Imaging Facility was used to obtain high resolution three-dimensional images of each knee, individually. The x-ray settings selected were determined by a 25 μm field of view, high resolution scan. Each scan ran for 14 minutes.

After scanning, all raw data was used to generate 3D volume data with a 4.5 μm^3 voxel size with Quantum GX software (Perkin Elmer Inc, Waltham, MA, USA). The number of slices per 3D image were determined based on the size of the knee and were limited to include mid-femoral shaft, mid-tibial shaft, and mid-fibular shaft (where possible). The ROI covered by the slices were centered on the deepest point of the femoral notch in both coronal and sagittal views.

Analyze 12.0 (Analyze Direct Inc., Overland Park, KS, USA) was used to obtain BMD, TJBV, and subchondral bone thickness. Each TJBV measurement was taken in the Analyze 12.0 ROI function, and limited to 30 slices (135 μm) beyond the epiphysis into the metaphysis on each bone. No part of the joint was excluded from this measurement. BMD was measured through the Analyze 12.0 Bone Microarchitecture Analysis (BMA) Add-On. The measurement was limited to 30 slices beyond the epiphysis into the metaphysis, but measurement of the growth plate was excluded.

Subchondral bone thickness was divided into four quadrants: medial femoral condyle, lateral femoral condyle, medial tibial plateau, and lateral tibial plateau. A linear ruler was used on 2D x-ray slice images generated from the sub-volume reconstruction. Measurements were taken

and averaged from three different images, spanning 20 slices. This ROI was determined based on the first image that had both medial and lateral sides visible for the respective bone.

3.1.5 *Knee Histology*

After μCT imaging was obtained, all paired knee samples (n=37) were fixed in 10% NBF for 24 hours followed by 70% ethanol for 3 days. Knees were fixed with the joint at 90-degrees flexion for proper coronal sectioning. De-calcification was performed by the Purdue Research Histology Laboratory using 25% formic acid and 10% sodium citrate solution. Four-micron, paraffin sections were processed and stained by the Purdue Research Histology Laboratory for H&E, SOFG, and F4/80+ macrophages.

Three blinded graders evaluated synovium and joint articular cartilage using H&E and SOFG stains, respectively. The synovial grading scheme, Modified Krenn Score, was used as previously published (Lewis et al., 2011). The Modified Mankin grading scheme was used for the articular cartilage evaluation, also as previously published (Furman et al., 2007).

F4/80+ stained synovium was analyzed using Olympus Count & Measure as previously described for the gut sections (Section 3.1.3). New thresholds were determined for differentiating positive F4/80+ staining from counter staining. The ROI for these sections was identified by the synovial reflection in all four quadrants of the knee: medial femur, lateral femur, medial tibia, and lateral tibia. Each synovium was outlined and terminated where the synovium reached the meniscus. AF ROI and ROC were obtained for each quadrant, as well.

3.1.6 *Statistics*

All results were analyzed with non-parametric comparisons across experimental groups. An each-pair Wilcoxon test was applied for all comparisons at a threshold of $p=0.05$ for significance. When control and operated limbs were taken into account, we focused on comparison across group operated limbs or within group comparisons.

3.2 Chronic Social Stress and Osteoarthritis Results

3.2.1 *Cytokines*

Of the 31 cytokines evaluated, seven concentrations showed significant changes. Eotaxin and G-CSF both showed higher median values in DMM+SD mice compared to Sham. Eotaxin, however, was only significantly higher when compared to Sham, while G-CSF in DMM+SD was significantly higher when compared to both DMM and Sham. Surprisingly, cytokines including IL-3, IL-5 and CXCL10 showed DMM+SD mice had significantly lower levels compared to mice with only DMM surgery. IL-5, IL-6, and CXCL1 in DMM+SD were significantly lower when compared to Sham. Eotaxin, IL-6 and CXCL1 in DMM+SD were not statistically significant compared to DMM surgery mice. All seven cytokines are shown in Figure 2.

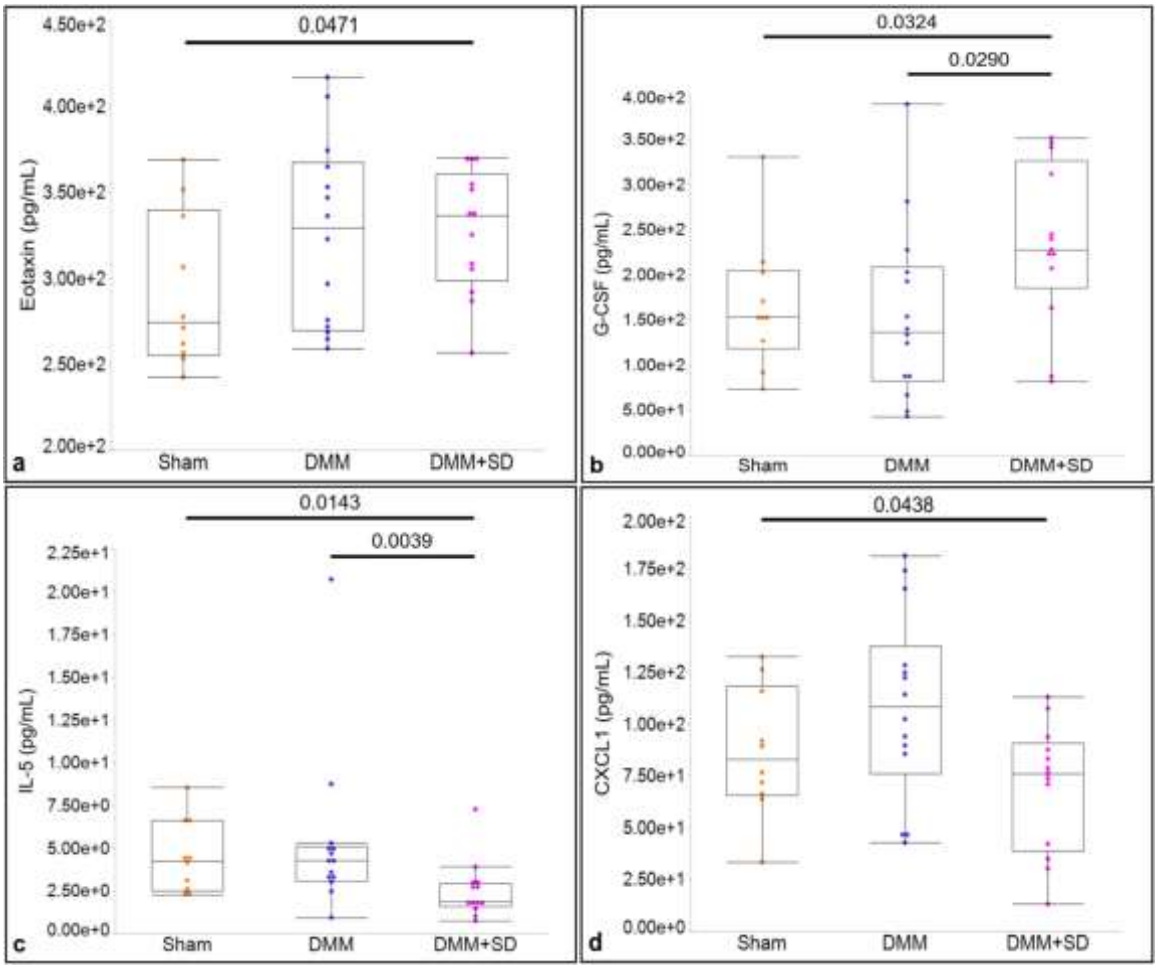

Figure 2. Levels of serum cytokines by group ($p<0.05$); a) Eotaxin concentration; b) G-CSF concentration; c) IL-5 concentration; d) CXCL1 concentration; e) IL-3 concentration; f) IL-6 concentration; g) CXCL10 concentration.

Figure 2. Levels of serum cytokines by group continued.

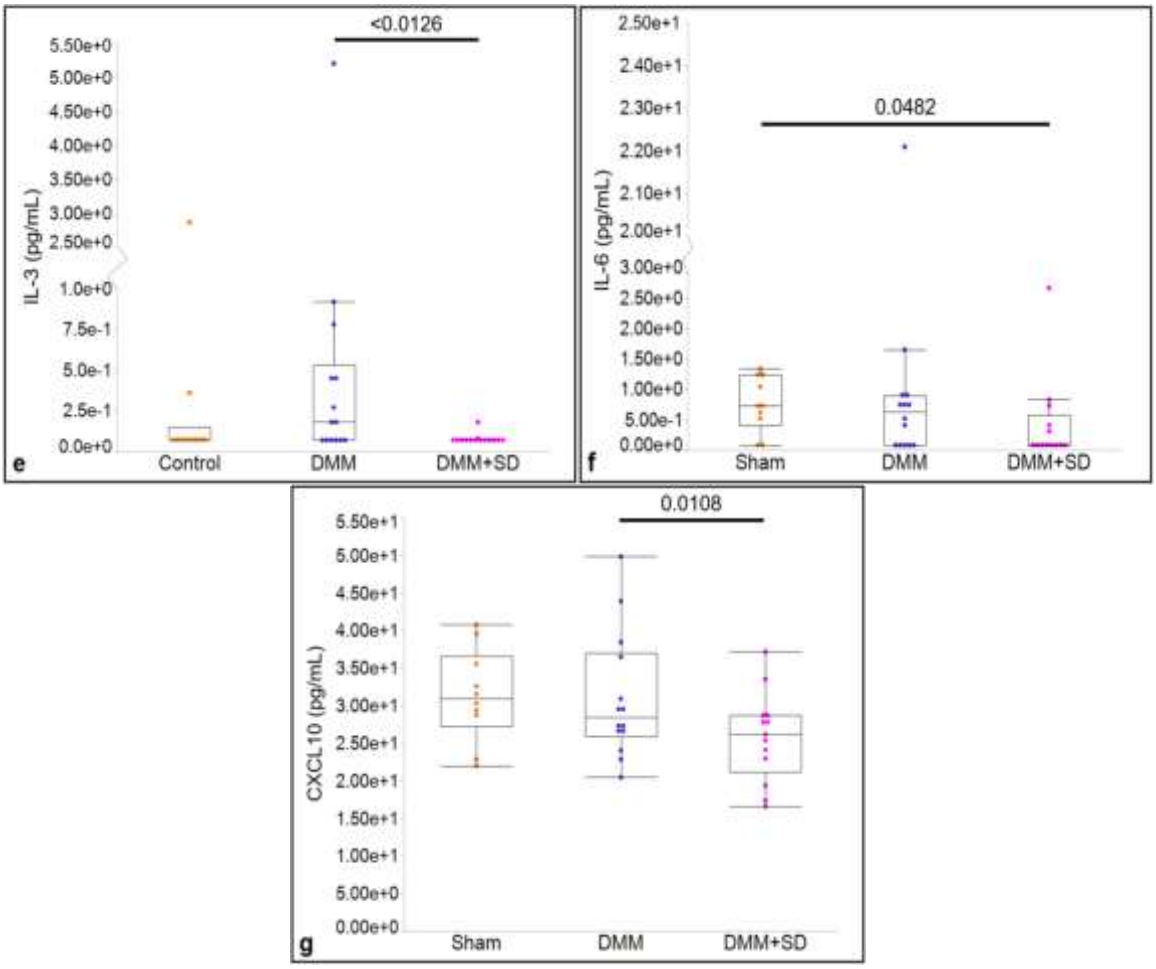

Serum creatinine and urine creatinine values (not reported individually) were used alongside B.Wt and BSA of the mice to obtain values approximating creatinine clearance by the kidneys. Creatinine clearance was of interest because of its importance as a biomarker of kidney function. When elevated, serum creatinine indicates decreased glomerular filtration rate, associated with impaired kidney function (Hokamp & Nabity, 2016; Yerramilli, Farace, Quinn, & Yerramilli, 2016). Given the unexpected decrease in some cytokines when comparing DMM+SD to DMM or Sham, we wanted to compare serum values to values normalized to B.Wt and creatinine ratios. By doing so we hoped to evaluate the impact of animal size and renal impairment on the cytokines and find additional support for the changes we were seeing. (UCreat:SCreat)/BSA, specifically, was used as a surrogate measure of creatinine clearance. A direct calculation of creatinine clearance was not possible because we did not have a measurement of urine output/24 hours.

Three additional calculations were performed: normalization to body weight, normalization to UCreat:SCreat, and normalization to (UCreat:SCreat)/BSA. Of these calculations, many changes were observed across groups in both pattern and significance values. Namely, of the seven cytokines that originally had significant concentration differences, only four cytokines maintained significance with all three normalization methods: eotaxin, G-CSF, IL-5, and CXCL1 (Figure 3). Within these four, eotaxin was the only cytokine that changed patterns based on normalization method, indicating it was likely affected most by creatinine clearance. It is also interesting to note that after creatinine clearance was taken into account, eotaxin, IL-5, and CXCL1 each showed that DMM had the highest values compared to both Sham and DMM+SD. G-CSF was the only cytokine to remain elevated in DMM+SD compared to DMM and Sham. To better visualize these changes, Figure 3 includes the original concentrations also shown in Figure 2.

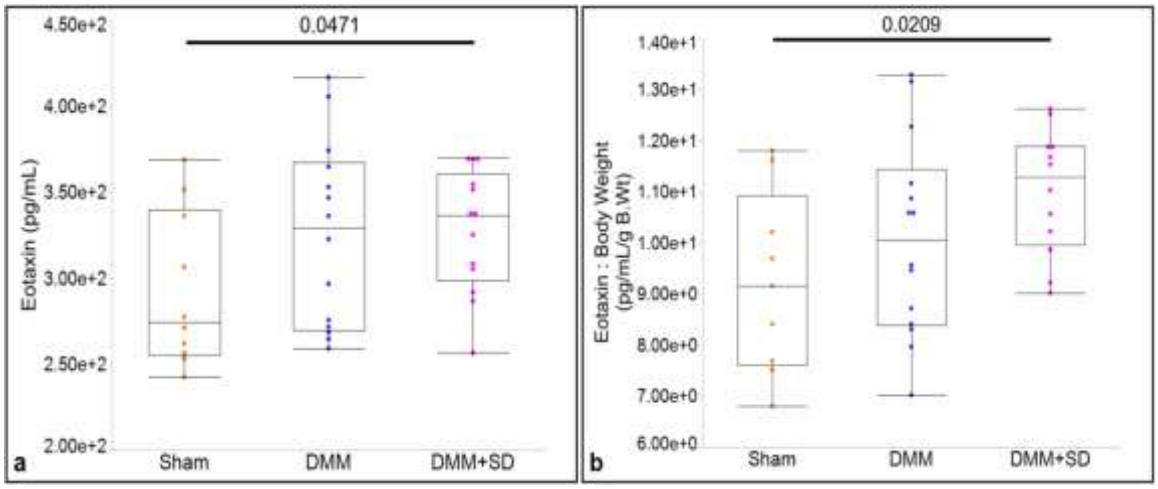

Figure 3. Levels of serum cytokines by group with different normalization methods ($p<0.05$); a) Serum eotaxin concentration; b) Serum eotaxin normalized to body weight (B.Wt) in grams; c) Serum eotaxin normalized to U Creat/S Creat; d) Serum eotaxin normalized to (U Creat/S Creat)/BSA; e) Serum G-CSF concentration; f) Serum G-CSF normalized to B.Wt in grams; g) Serum G-CSF normalized to U Creat/S Creat; h) Serum G-CSF normalized to (U Creat/S Creat)/BSA; i) Serum IL-5 concentration; j) Serum IL-5 normalized to B.Wt in grams; k) Serum IL-5 normalized to U Creat/S Creat; l) Serum IL-5 normalized to (U Creat/S Creat)/BSA; m) Serum CXCL1 concentration; n) Serum CXCL1 normalized to B.Wt in grams; o) Serum CXCL1 normalized to U Creat/S Creat; p) Serum CXCL1 normalized to (U Creat/S Creat)/BSA.

Figure 3. Levels of serum cytokines by group with different normalization methods continued.

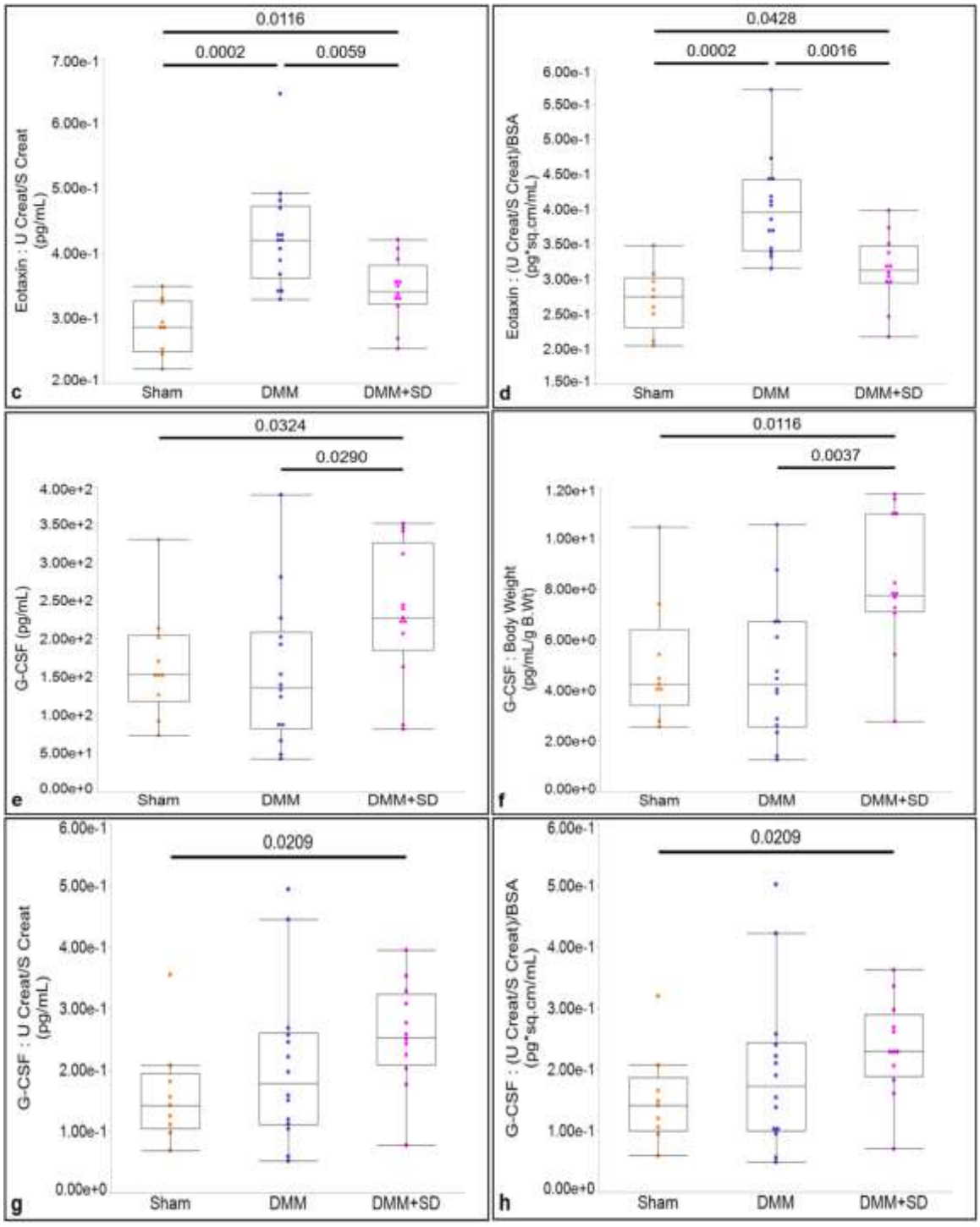

Figure 3. Levels of serum cytokines by group with different normalization methods continued.

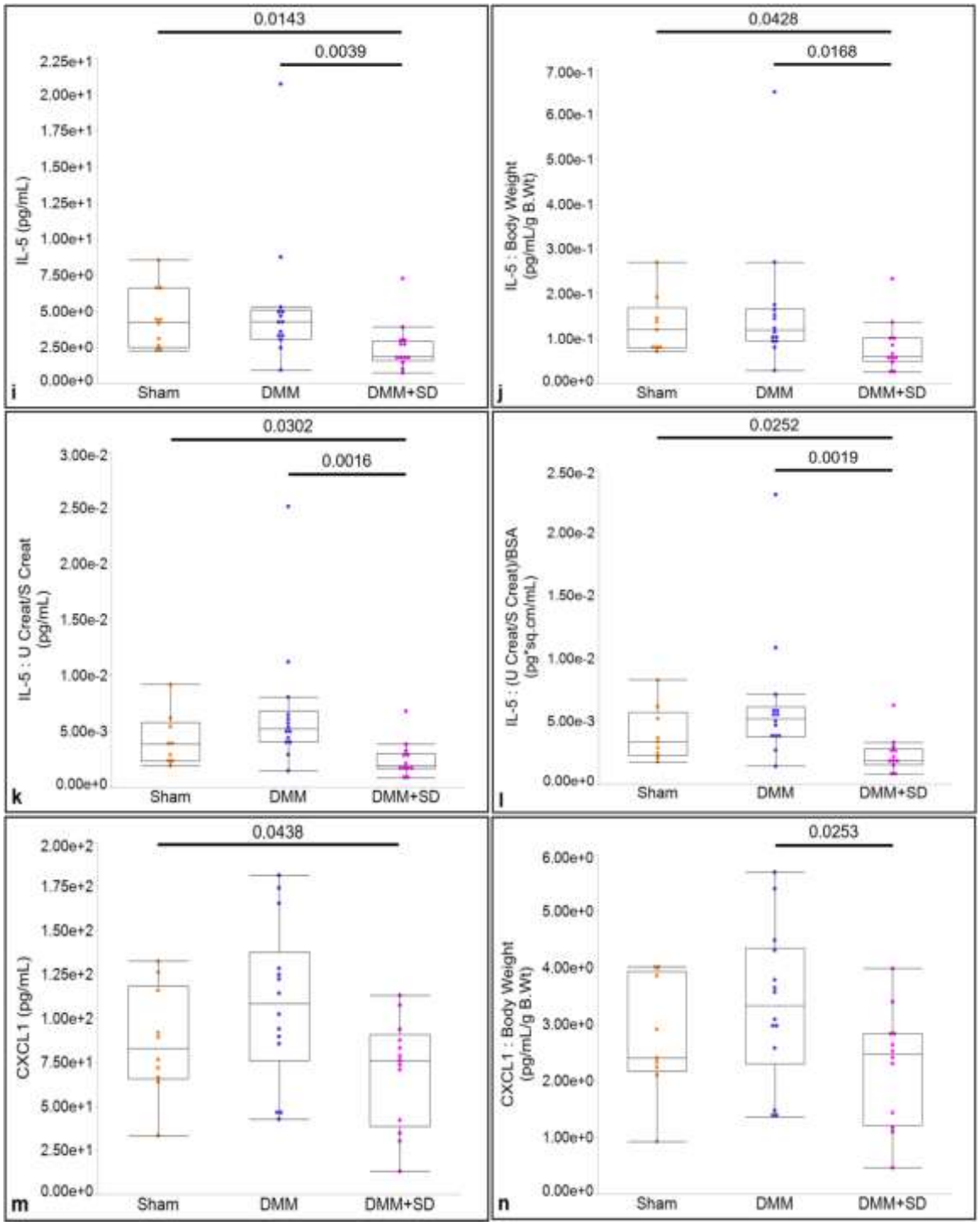

Figure 3. Levels of serum cytokines by group with different normalization methods continued.

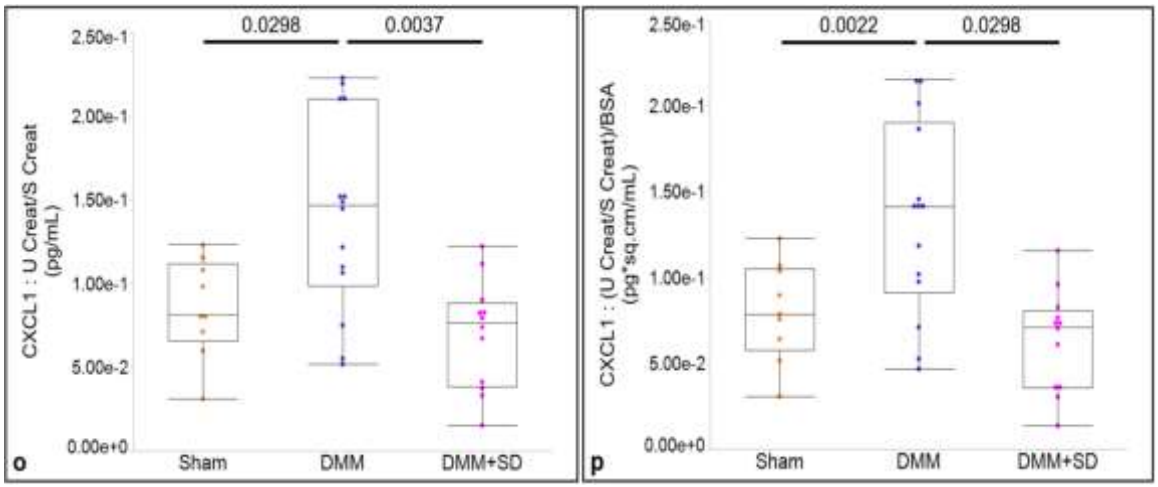

3.2.2 *Stress Biomarkers*

As expected, there was significantly increased serum corticosterone found in DMM+SD when compared to Sham mice. There was no statistical significance between DMM and DMM+SD, but there was a trend to increase in corticosterone for DMM compared to Sham mice. Figure 4a shows this pattern of increasing corticosterone across groups. This pattern was maintained when considering body weight normalization, but the pattern reflects similar to previous cytokines noted after UCreat:SCreat and (UCreat:SCreat)/BSA were taken into account (Figure 4b-d). DMM+SD had significantly lower corticosterone values compared to DMM after (UCreat:SCreat)/BSA normalization. To assess if corticosterone was excreted into the urine at greater levels in DMM+SD compared to DMM, urinary corticosterone ELISA was attempted, but the results were not significant (data not shown).

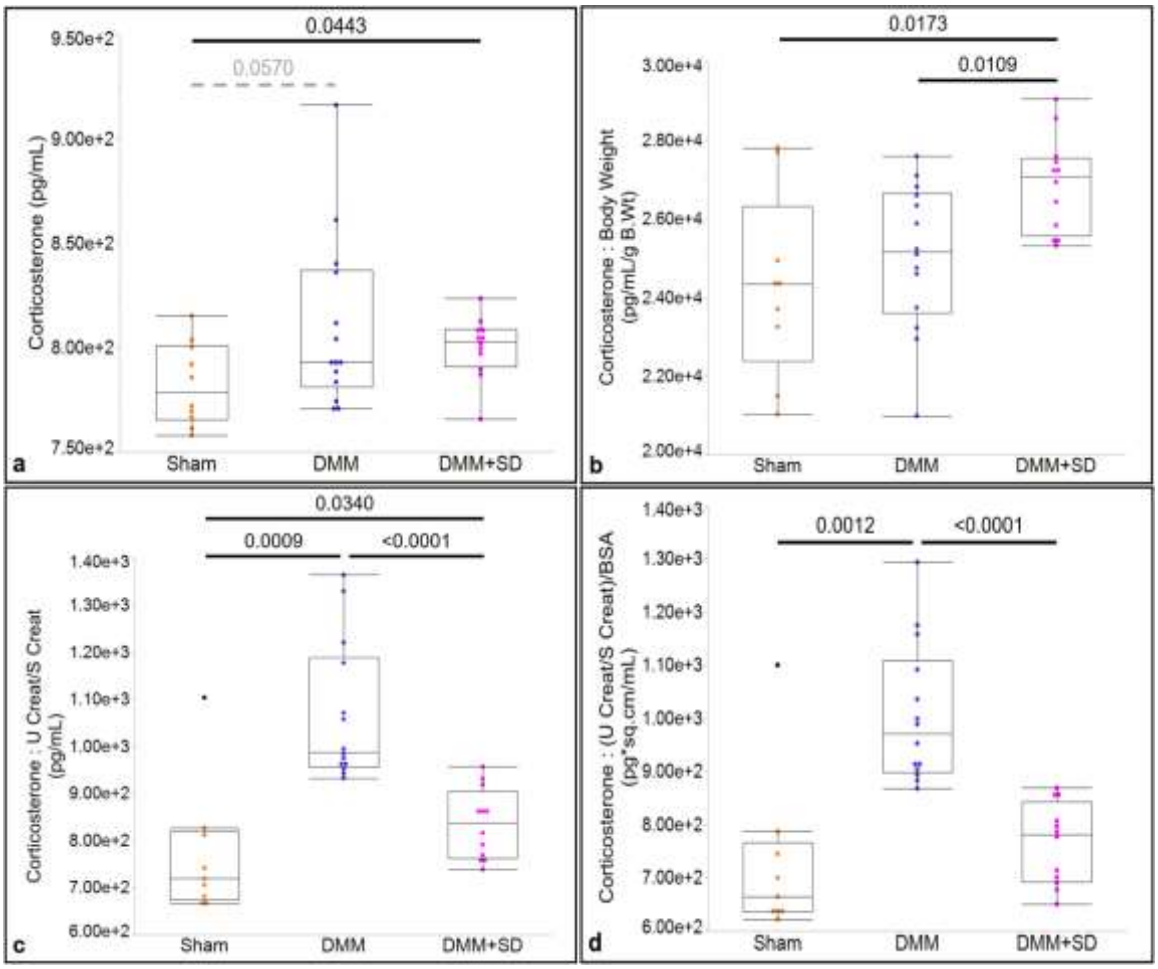

Figure 4. Levels of serum corticosterone by group with different normalization methods ($p<0.05$); a) Serum corticosterone concentration; b) Serum corticosterone normalized to body weight in grams; c) Serum corticosterone normalized to U Creat/S Creat; d) Serum corticosterone normalized to (U Creat/S Creat)/BSA.

BDNF was measured in the pituitary array performed by Eve Technologies. This value was observed as a biomarker for depression-like disorders (Bathina & Das, 2015). The results of this test, however, were below detectable limit and could not be evaluated.

3.2.3 *Osteoarthritis Biomarker (CTX-II)*

Serum and urine CTX-II were measured by ELISA as a biomarker for OA development (Duclos et al., 2010). Serum CTX-II levels were not different across experimental groups. After body weight normalization and creatinine parameter normalizations, DMM+SD levels were altered by an increase and then decrease, respectively. This is consistent with the pattern changes

we have seen across normalization methods, thus far. Figure 6 shows these patterns for serum CTX-II.

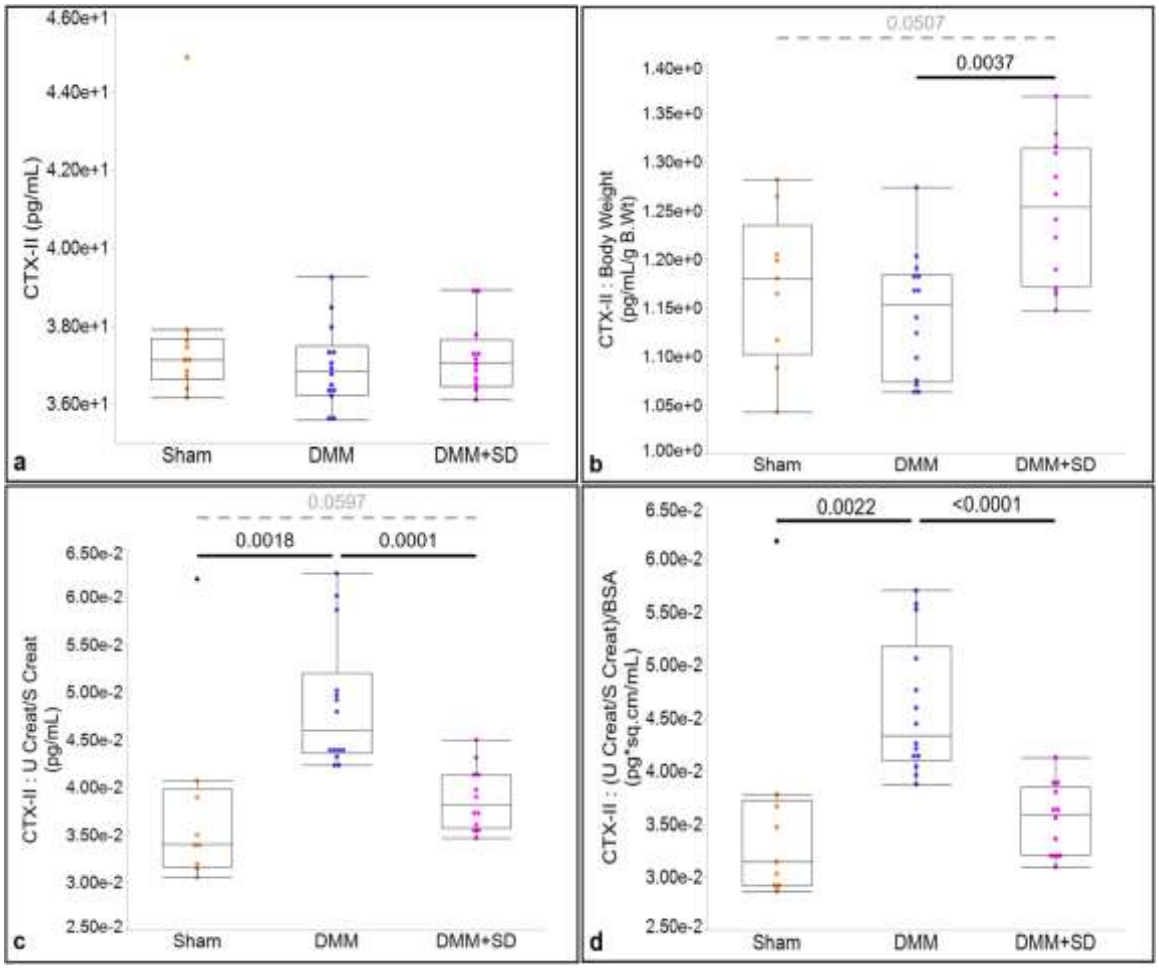

Figure 5. Levels of serum CTX-II by group with different normalization methods ($p<0.05$); a) Serum CTX-II concentration; b) Serum CTX-II normalized to body weight in grams; c) Serum CTX-II normalized to U Creat/S Creat; d) Serum CTX-II normalized to (U Creat/S Creat)/BSA.

Urinary CTX-II also did not show significant differences across groups or after UCreat:SCreat ratio normalization. Both body weight normalization and (UCreat:SCreat)/BSA showed significant differences between DMM and DMM+SD. Urinary CTX-II normalized to body weight showed higher DMM+SD compared to DMM while the (UCreat:SCreat)/BSA normalization showed the opposite. Figure 7 below shows the urinary CTX-II results with different normalization methods.

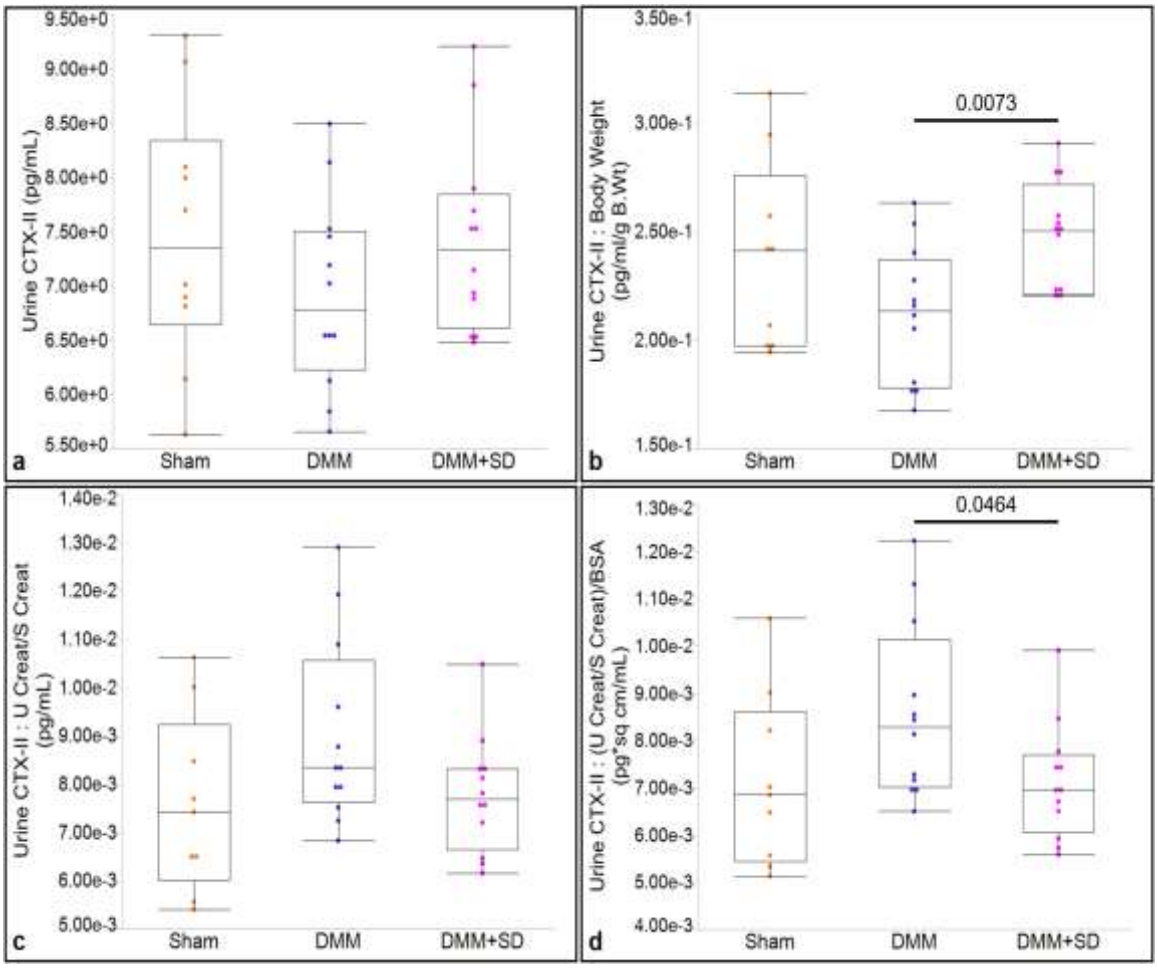

Figure 6. Urine CTX-II by group with different normalization methods ($p<0.05$); a) Urine CTX-II concentration; b) Urine CTX-II normalized to body weight in grams; c) Urine CTX-II normalized to U Creat/S Creat; d) Urine CTX-II normalized to (U Creat/S Creat)/BSA.

3.2.4 *Gastrointestinal Histology*

Each section of gastrointestinal tract was evaluated for percent macrophage infiltration as an estimate for overall gut inflammation. Representative images of each gut section are shown in Figure 8 (on the next page).

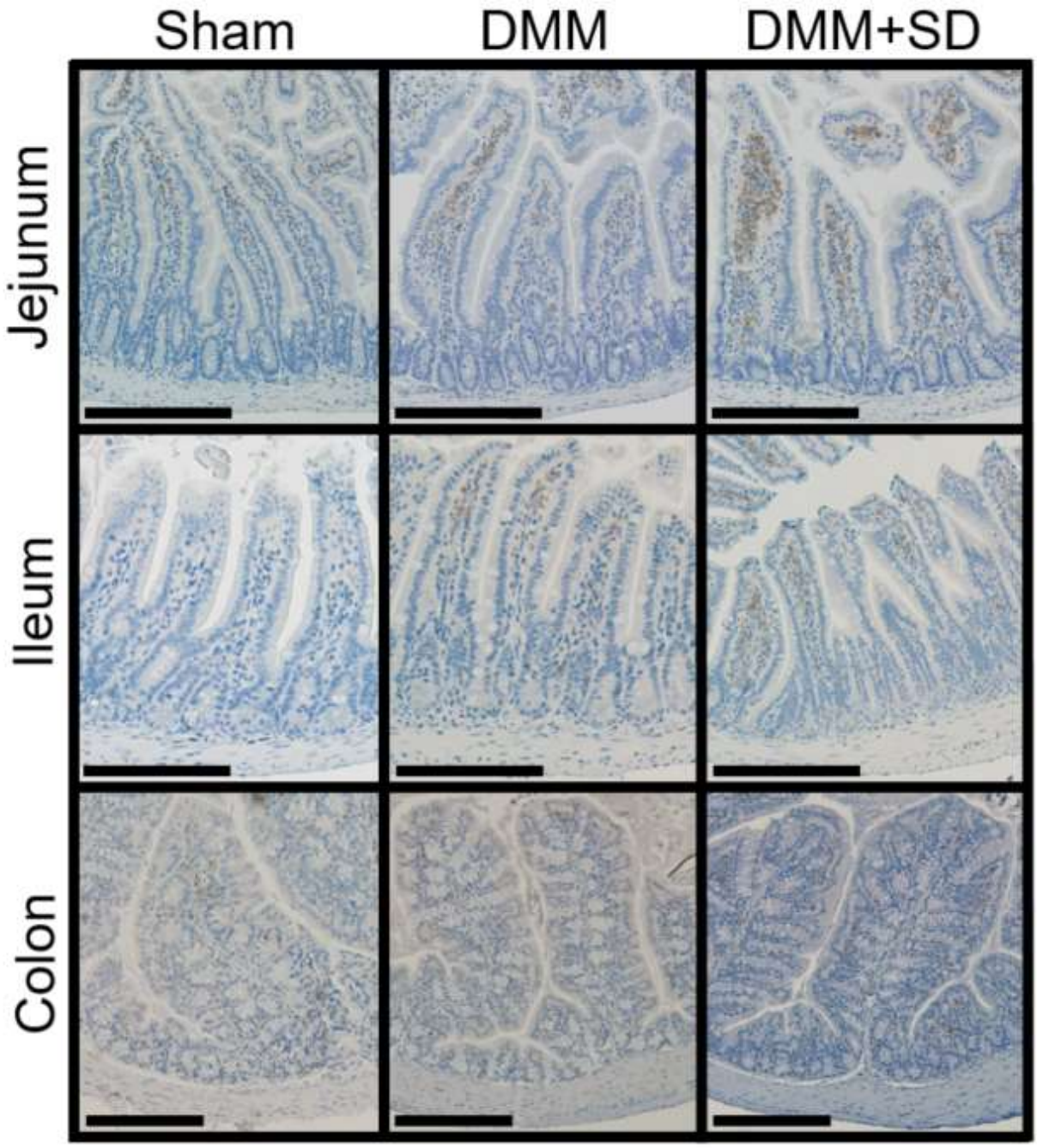

Figure 7. Representative images of gastrointestinal F4/80+ macrophage staining by group. Jejunum & Ileum Bars = 100 μm; Colon Bars = 200 μm.

Although there were no sections of gut that had significant differences in macrophages as a measure of percentage within a ROI, jejunum and ileum both had trends towards significance. For example, jejunum from DMM+SD mice had a trend to higher macrophage AF ROI, with p=0.0597, when compared to Sham mice. DMM mice also had a trend to higher macrophage AF

ROI, with p=0.0597, when compared to Sham. However, ileum sections from DMM+SD had a trend to lower AF ROI compared to DMM, with p=0.0606. Similar ROC trends also occurred, but no significance was found with a threshold of $p<0.05$ (data not shown). Colon did not show any differences between groups when considering either AF ROI or ROC. Figure 9 shows AF ROI compared across groups for each gut section.

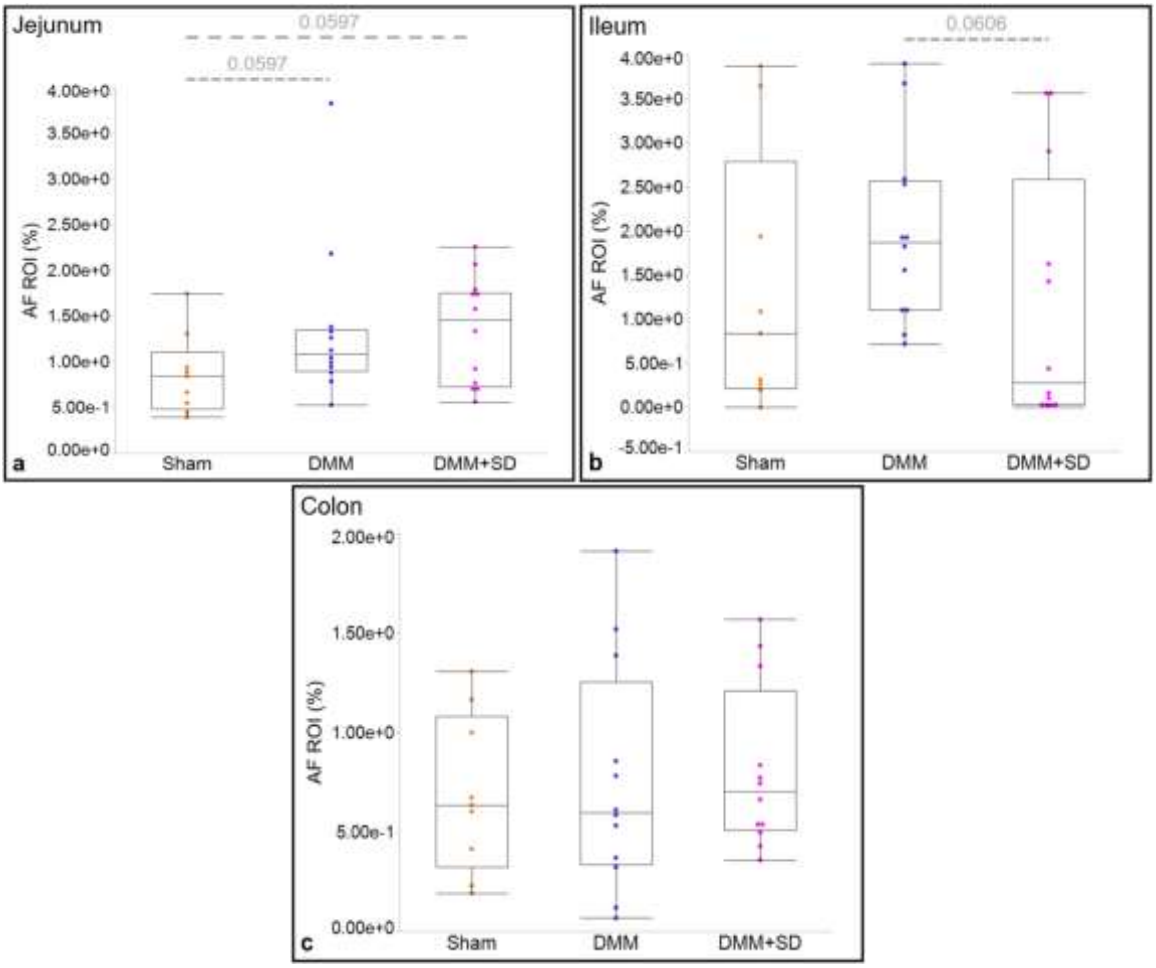

Figure 8. Area fraction of region of interest (AF ROI) of F4/80+ macrophages by group ($p<0.05$); a) AF ROI of jejunum; b) AF ROI of ileum; c) AF ROI of colon.

3.2.5 *Knee μCT*

TJBV, BMD, and subchondral bone thickness were measured as indicators of OA. Representative μCT 3D images are shown in Figure 10 with comparison between operated limb and control limb. Figure 11 shows the TJBV values. Notably, there were no significant differences between TJBV of any experimental group, but both DMM+SD and DMM mice had significantly higher TJBV in their operated limb compared to their contralateral control limb.

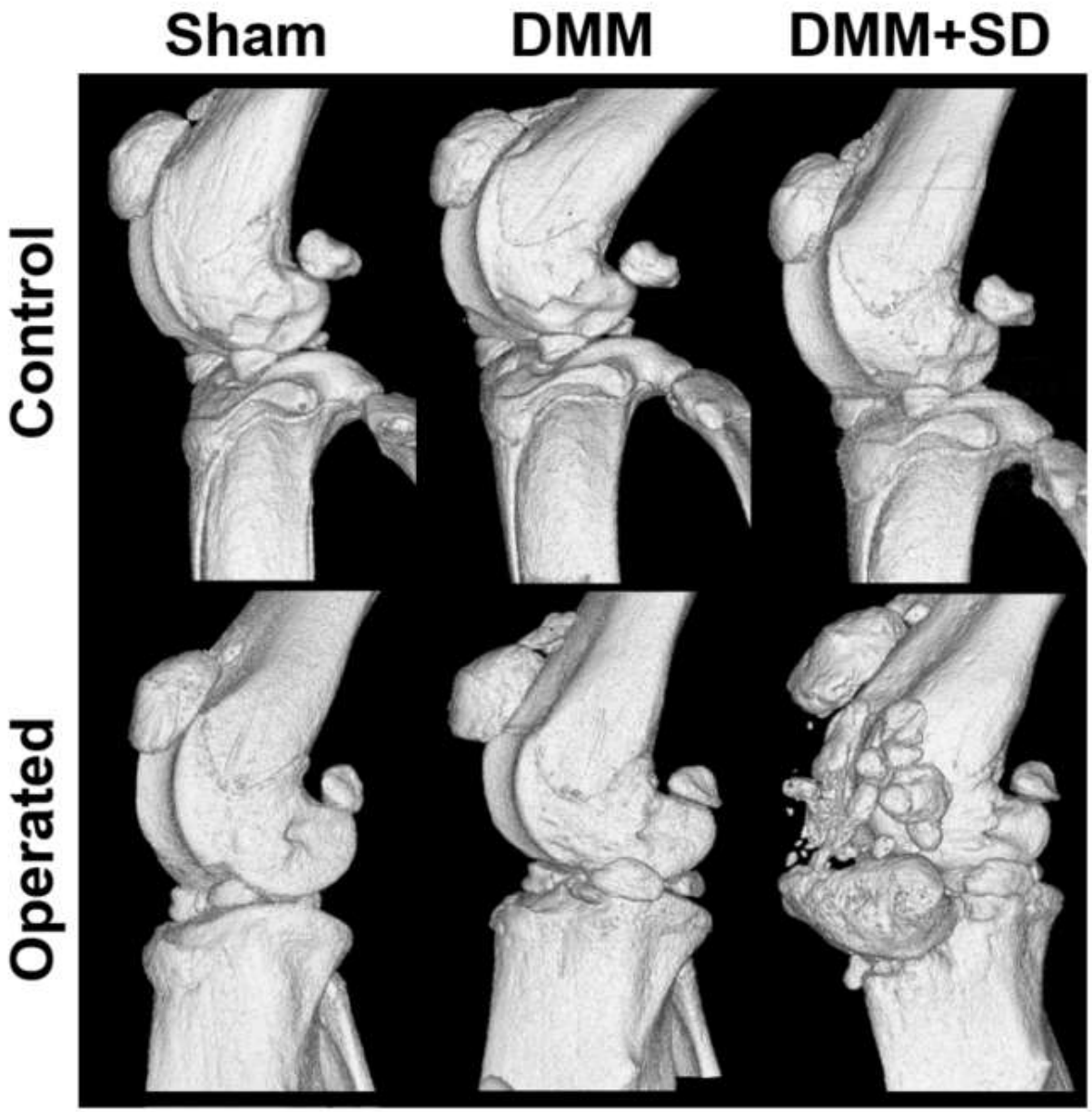

Figure 9. Representative μCT images by group.

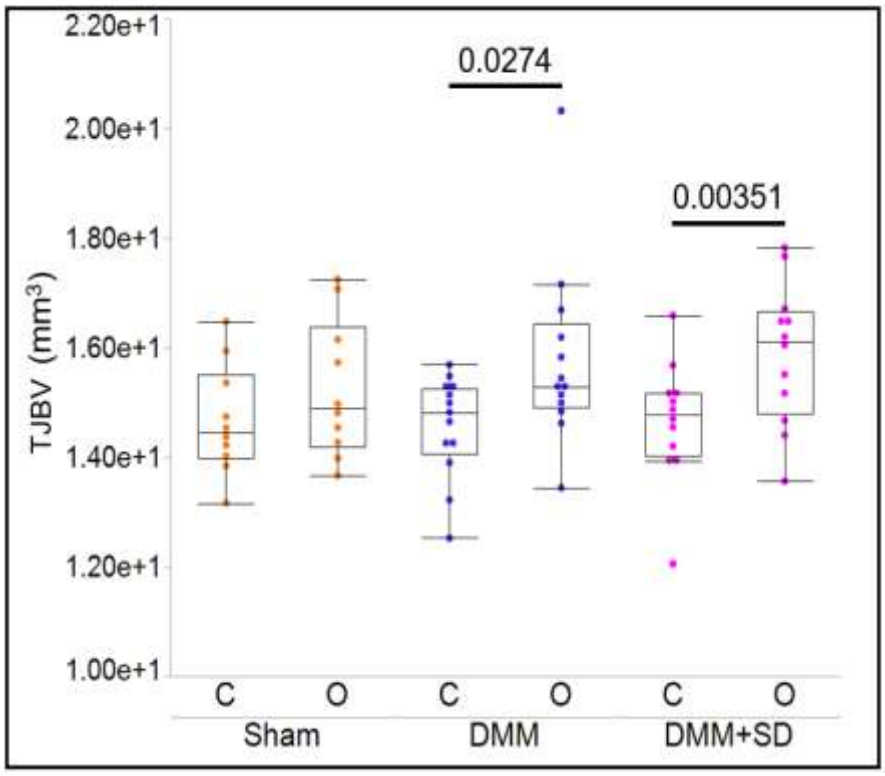

Figure 10. Total joint bone volume (TJBV) by group ($p<0.05$). C = control limb; O = operated limb.

There were no significant differences in BMD for femur or tibia between groups. There were no significant differences between control and operated limbs in any group. Figure 12 shows the two graphs representing these data.

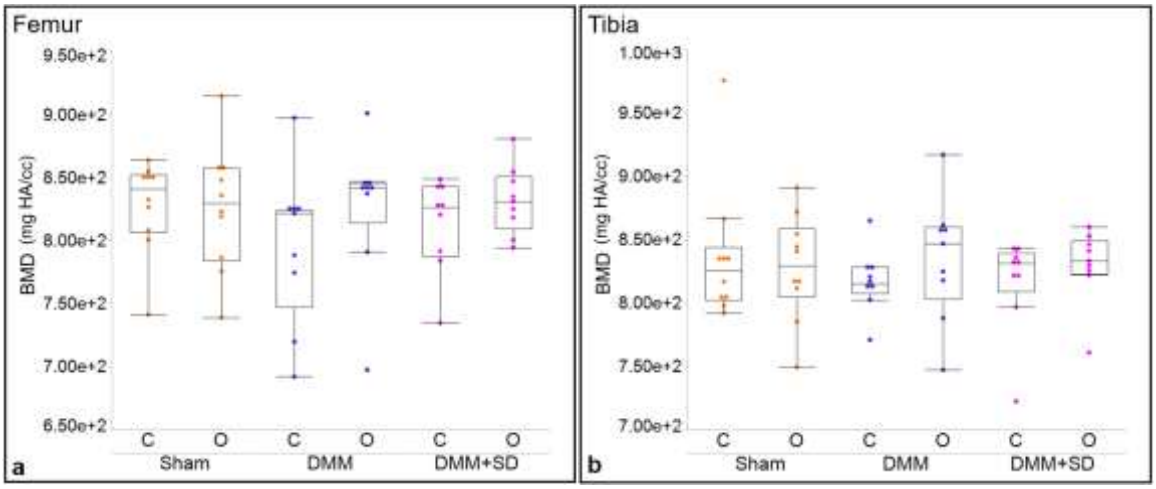

Figure 11. Bone mineral density (BMD) by group ($p<0.05$). C = control limb; O = operated limb; a) Femur BMD; b) Tibia BMD.

The medial femur was the only joint quadrant to show significant differences across groups with measured subchondral bone thickness. More specifically, DMM operated limbs had significantly increased subchondral bone thicknesses compared to DMM+SD operated limbs, and Sham operated limbs were significantly increased compared to DMM+SD operated limbs. There was a significant difference between control and operated limbs of DMM, and DMM+SD mice had a trend towards significance (p=0.0638). Figure 13 outlines subchondral bone thickness by quadrant.

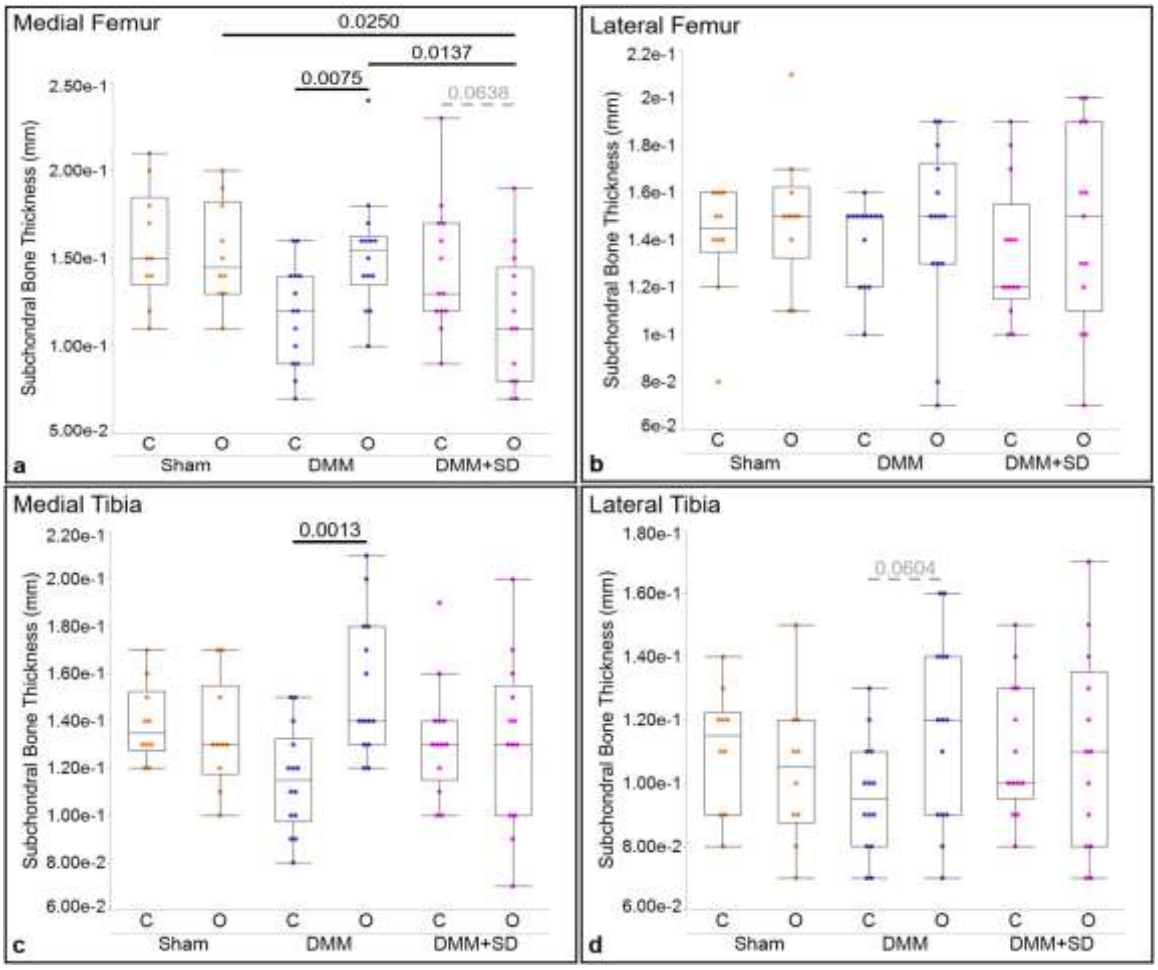

Figure 12. Subchondral bone thickness by group ($p<0.05$); a) Subchondral bone thickness medial femur; b) Subchondral bone thickness lateral femur; c) Subchondral bone thickness medial tibia; d) Subchondral bone thickness lateral tibia; C = control limb; O = operated limb.

3.2.6 *Knee Histology*

SOFG staining was evaluated on knee joints in order to assess the degree of structural OA, while H&E staining was evaluated to assess synovial membrane thickening. Figure 14 and Figure

15 show representative images highlighting the area scored for each structural OA evaluation and synovial membrane evaluation, respectively.

Figure 13. Representative knee coronal sections and regions of interest stained with SOFG for OA grading. Bar in center pane = 200 μm; Bar in projections = 100 μm.

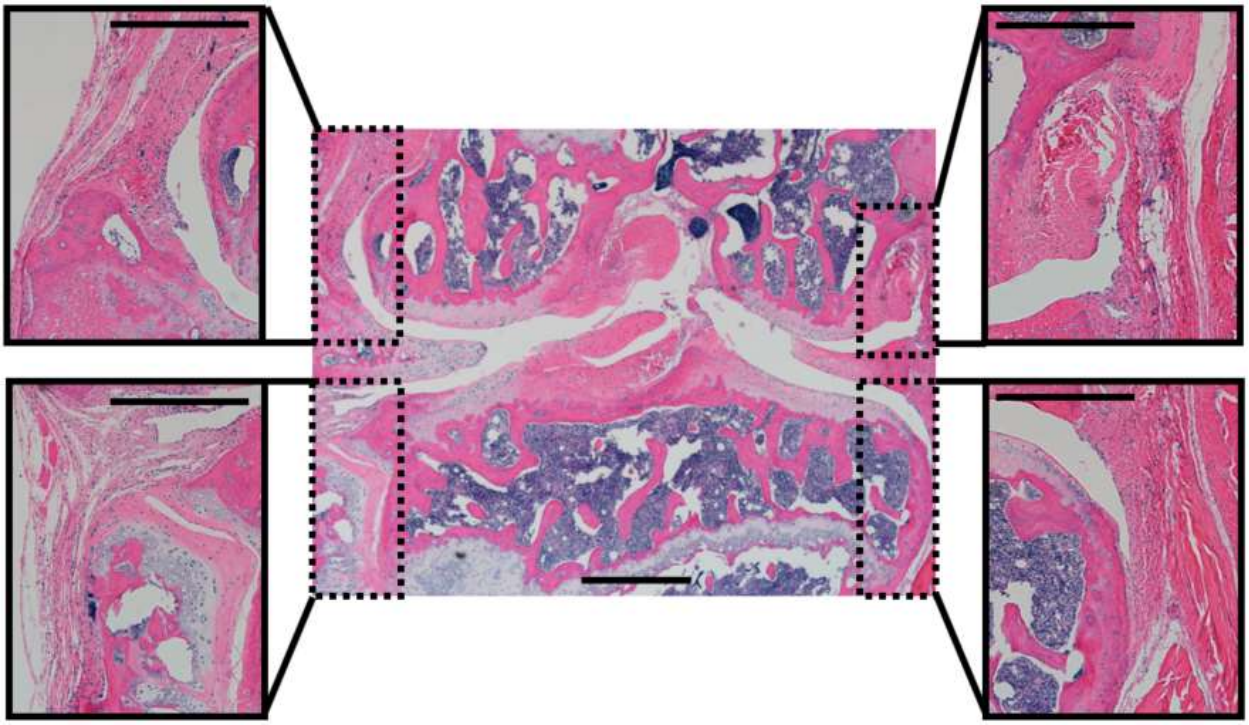

Figure 14. Representative knee coronal sections and regions of interest stained with H&E for synovitis grading. Bar in center pane = 200 μm; Bar in projections = 100 μm.

When considering the total joint score for OA, DMM+SD had significantly higher scores than Sham, and DMM also had significantly higher scores than Sham. DMM+SD and DMM were not statistically different from one another, but the total joint score of the operated DMM and Sham limbs were significantly different compared to the control limb (Figure 16). When evaluating individual quadrants, all comparisons were the same within medial femur and medial tibia. These changes are reflected in Figure 17. The patterns noted in OA total joint score were the same across all quadrants.

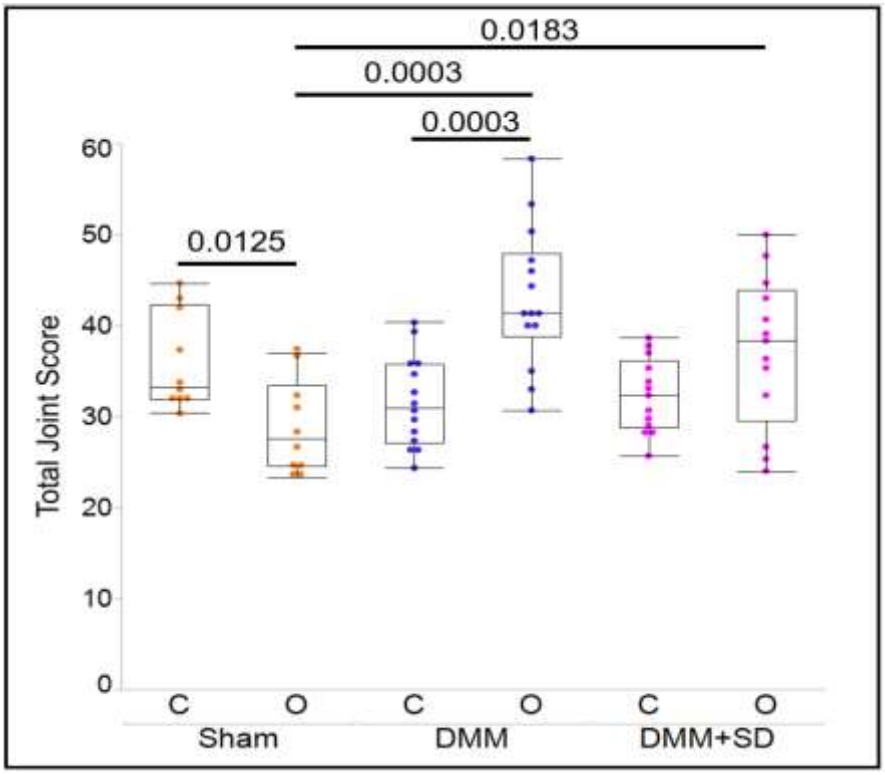

Figure 15. Osteoarthritis total joint score ($p<0.05$); C = control limb; O = operated limb.

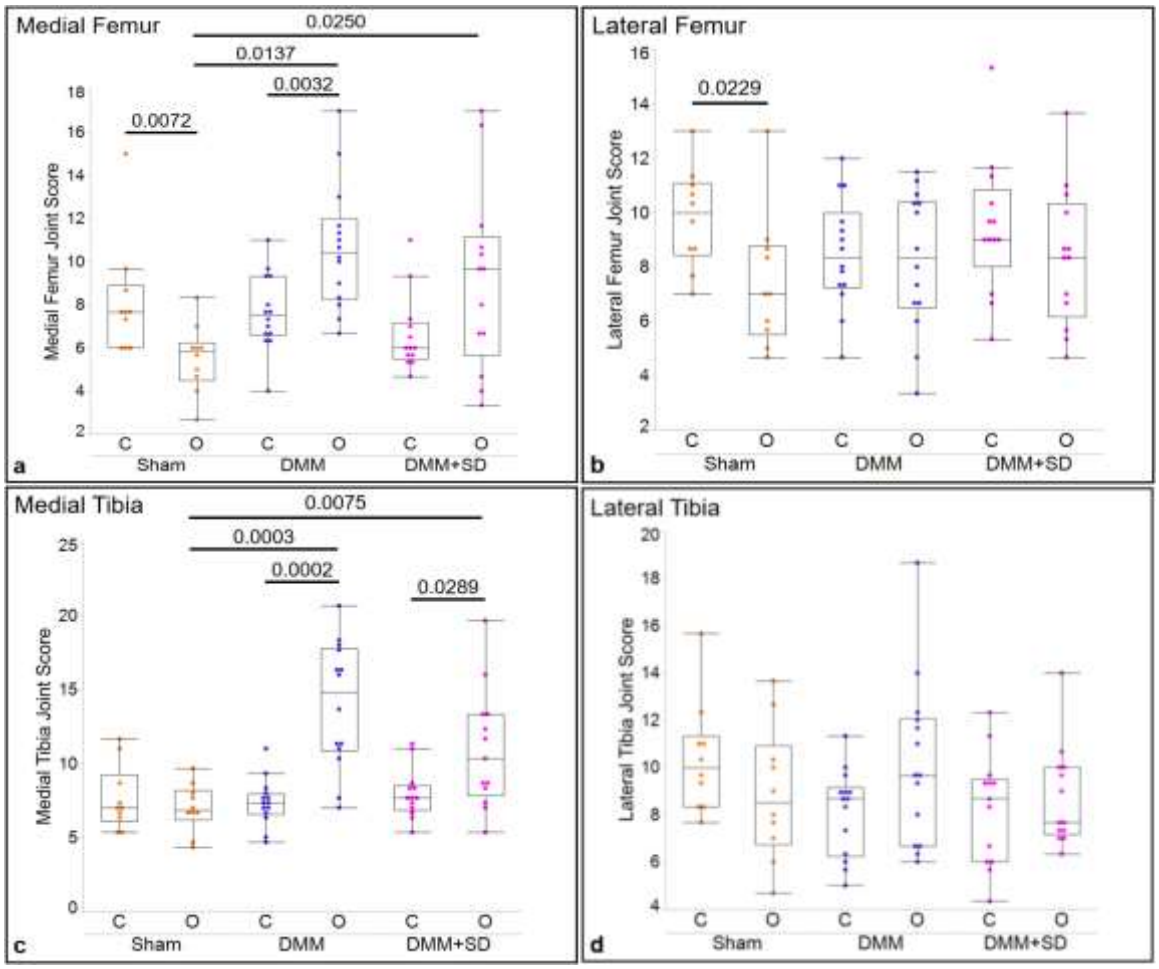

Figure 16. Osteoarthritis joint score by quadrant ($p<0.05$); C = control limb; O = operated limb; a) Osteoarthritis score for medial femur; b) Osteoarthritis score for lateral femur; c) Osteoarthritis score for medial tibia; d) Osteoarthritis score for lateral tibia.

Overall, the total joint score of synovitis for the operated limb was significantly higher in DMM+SD mice compared to Sham mice. DMM mice also had significantly higher scores compared to Sham. DMM mice had significantly higher total joint score in their operated limb compared to their control limb, while DMM+SD had a trend towards significance (Figure 18). When considering individual quadrants with synovitis scoring, all quadrants showed significantly higher DMM scores compared to Sham scores. Medial and lateral tibia also showed significantly higher DMM+SD compared to Sham operated limbs. Figure 19 outlines the synovitis scores by quadrant.

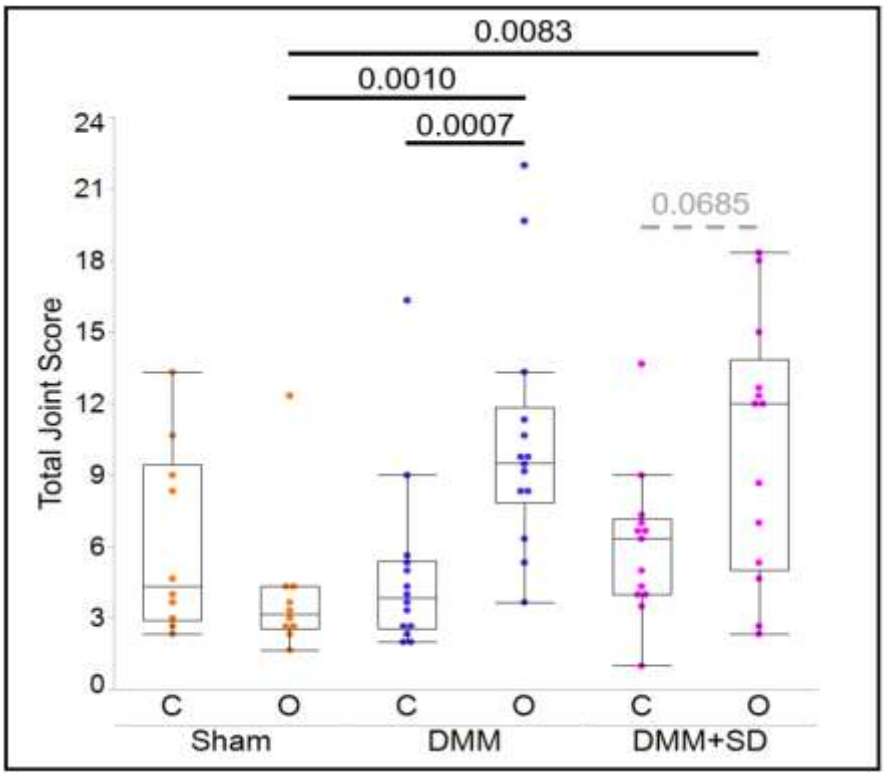

Figure 17. Synovitis total joint score ($p<0.05$); C = control limb; O = operated limb.

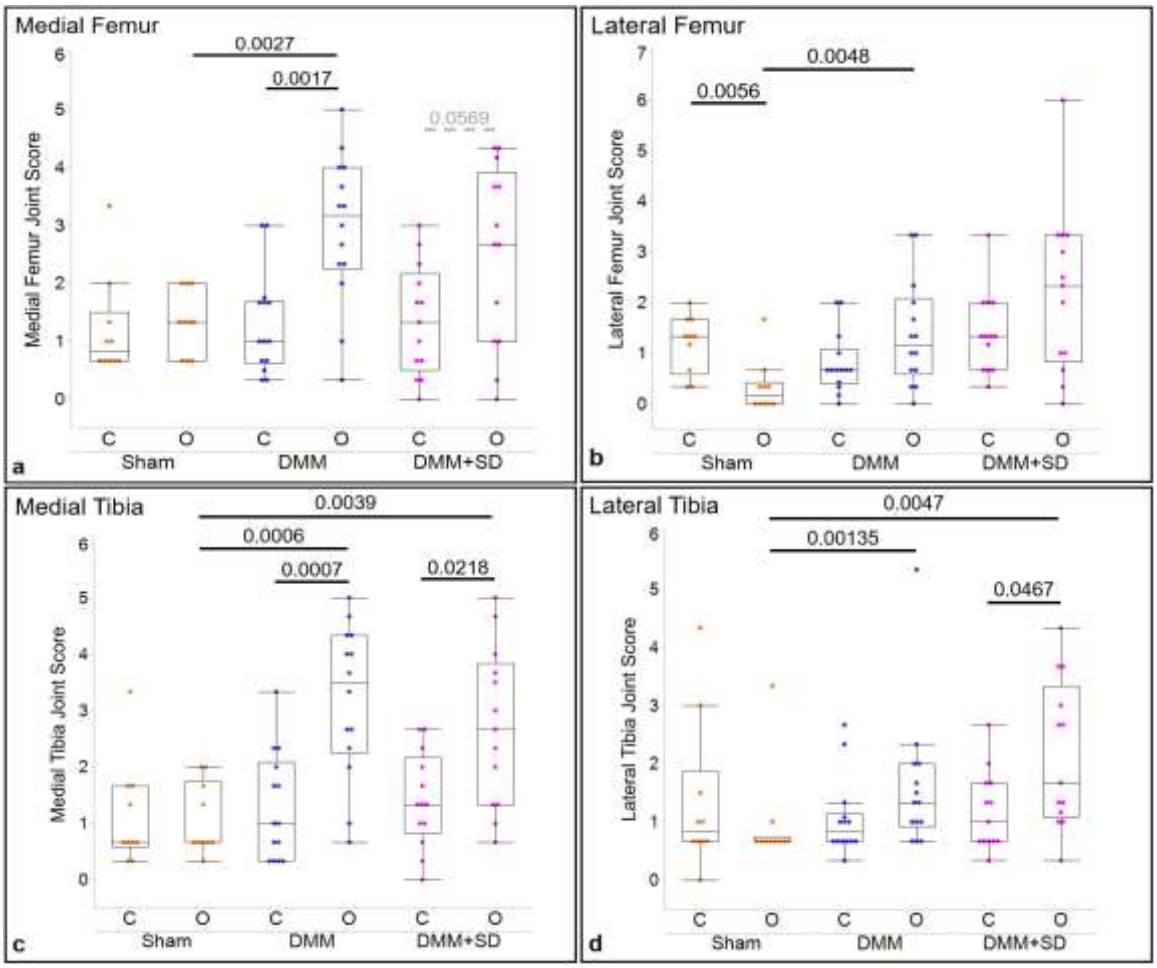

Figure 18. Synovitis joint score by quadrant ($p<0.05$); C = control limb; O = operated limb; a) Synovitis score for medial femur; b) Synovitis score for lateral femur; c) Synovitis score for medial tibia; d) Synovitis score for lateral tibia.

F4/80+ staining was applied to knee joints to assess synovitis of each knee quadrant. Representative images of knee joints stained for F4/80+ macrophages are displayed in Figure 20. Values of AF ROI for all four quadrants are shown in Figure 21. There were no significant differences on the lateral side, but a trend towards increased F4/80+ expression occurred on the medial tibia. Here, operated DMM+SD limbs had a higher percentage of F4/80+ macrophage AF ROI, compared to operated DMM limbs, but Sham operated limbs also had increased expression compared to DMM. There was also a significant difference between operated limb of Sham mice compared to operated limb of DMM mice in the medial femur, with Sham mice having a higher median F4/80+ expression.

Figure 19. Representative coronal sections of regions of interest for F4/80+ immunohistochemistry. Bar in center pane = 200 μm; Bar in projections = 100 μm.

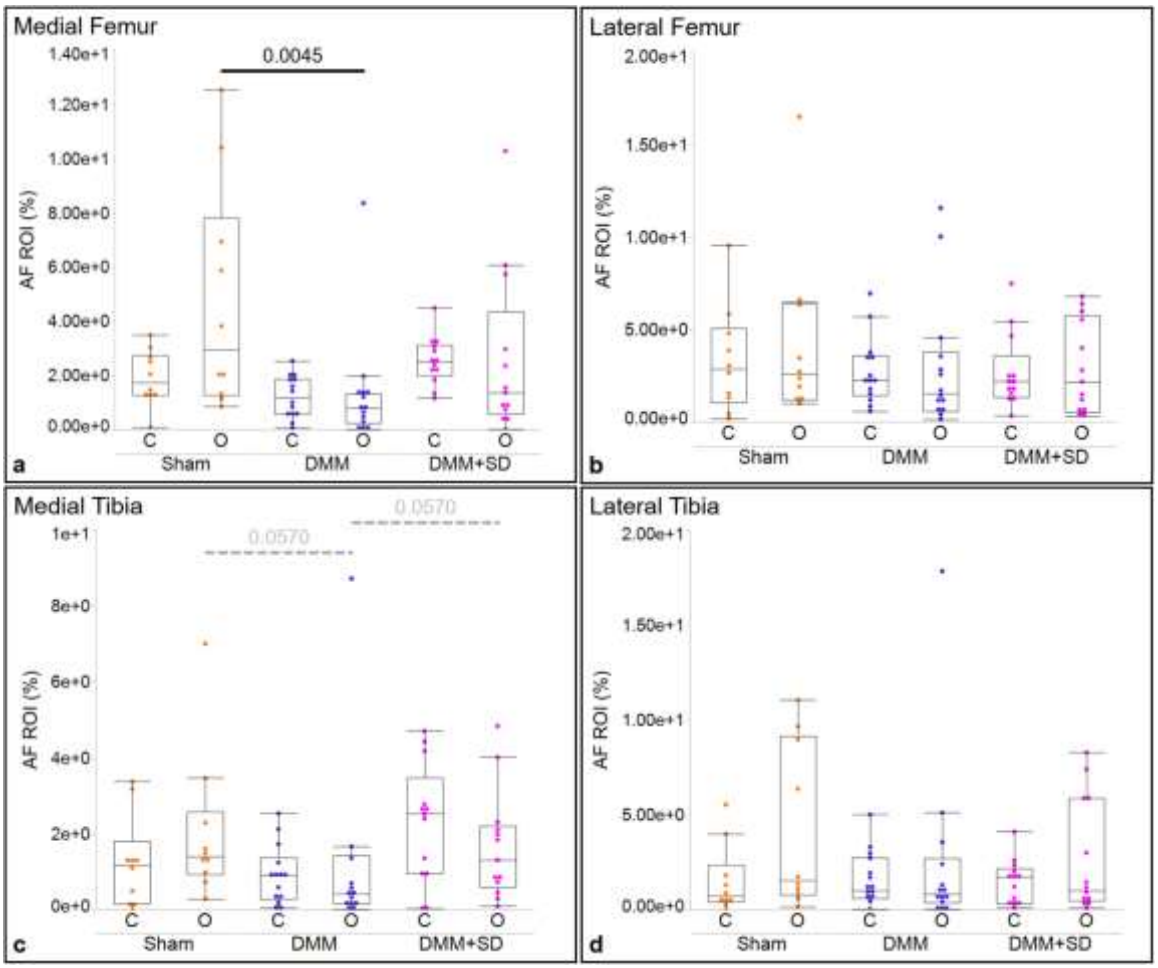

Figure 20. Area fraction of region of interest (AF ROI) of F4/80+ macrophages by group ($p<0.05$); C = control limb; O = operated limb; a) AF ROI of medial femur; b) AF ROI of lateral femur; c) AF ROI of medial tibia; d) AF ROI of lateral tibia.

3.3 Chronic Social Stress and Osteoarthritis Discussion

In the present study, we show the effects of chronic stress on the knee OA phenotype and systemic inflammation in mice with PTOA. Overall, we were able to show that chronic social stress does impact mice, but DMM+SD mice were impacted differently than expected compared to mice that only underwent DMM surgery or Sham surgery.

First and foremost, we were able to demonstrate that OA developed to a similar extent in both DMM and DMM+SD mice. This was shown through TJBV, histologic grading of articular cartilage, and histologic grading of synovium analysis (Figures 11, 16, and 18). While the differences we expected to see across groups were not always present, DMM mice and DMM+SD mice showed significant differences between control and operated limbs for several OA indicators.

For example, both DMM and DMM+SD mice had significantly higher TJBV in their operated limbs compared to control limbs. This is also apparent in the representative 3D images of the stifle joints where DMM has a small enlargement of the normally ossified medial meniscus and additional smaller osteophytes in the same area. DMM+SD shows much more obvious changes, including extensive osteophyte formation and calcification of the soft tissues surrounding the joint (Figure 10). Synovitis evaluation showed an increased Modified Krenn total joint score that was significantly higher or trending towards this difference when comparing control and operated limbs of DMM or DMM+SD. Degree of structural OA, however, can be better described by changes in the Modified Mankin articular cartilage evaluation. In this case, the total cartilage score for DMM+SD did not show a significant difference between control and operated limbs, but there was a significant difference when comparing DMM control and operated limbs. Additionally, the operated DMM+SD limb still had a significantly higher total score compared to the Sham operated limb. This supports OA development when taking into consideration that there were no indications Sham operated limbs developed OA (Figure 16). The lack of differences in BMD across groups was surprising (Figure 12), because in OA, we would expect increases in BMD due to increased bone remodeling (Cai et al., 2020). Several mice, however, had BMD of less than 800 mg HA/cc where typical BMD of mice ranges from 850 mg HA/cc to 930 mg HA/cc depending on bone (femur or tibia) and area of the bone (metaphysis or epiphysis) (Carballo et al., 2018). This suggests that contrary to our expectations, some mice had decreased BMD and were osteoporotic. This issue may arise from disuse or from chronic elevations in serum corticosterone (Komori, 2015, 2016).

CTX-II is well studied as a degradation product of type II collagen that dominates articular cartilage. Typically, serum CTX-II increases with worsened OA (Duclos et al., 2010). Neither serum nor urinary CTX-II concentration data demonstrated differences between DMM, or DMM+SD, mice compared to Sham surgery mice. However, after correcting for body weight, DMM+SD mice had significantly higher serum and urinary levels compared to DMM. On the contrary, both urinary and serum CTX-II had significantly lower levels in DMM+SD compared to DMM when normalized to (UCreat/SCreat)/BSA (Figure 6 and Figure 7).

Rabbit CTX-II levels initially peak of CTX-II two week post-operatively, likely corresponding with post-operative inflammation and increased collagen turnover. Six weeks post-operatively another increase is noted, with a peak at 12 weeks post-operatively. After the twelfth

week, there were progressive decreases for the remainder of the study (carried out for 20 weeks). The second peak has not been described in mice, to the best of our knowledge (Duclos et al., 2010). Rats also show differential levels of CTX-II depending on day post-operatively, where peak CTX-II is reached at two weeks (Nielsen et al., 2008). CTX-II has been correlated with oxidative stress markers in mice, even in the absence of significant differences in the overall level across experimental groups (Watari et al., 2011). Additionally, urinary CTX-II levels were not significantly different in mice with spontaneous OA, but did vary with the age of the mice. A peak urinary OA was noted in the mice 20 to 24 weeks of age (Sarukawa, Takahashi, Doi, Suzuki, & Nagano, 2010). Since our study did not see a significant difference in serum or urinary CTX-II, it could be due to the time-course of serum CTX-II or the impact of age on the marker. The serum from our mice were collected at 28-weeks of age, which was 12 weeks post-operative. Since neither showed elevations, it is likely we are seeing a lack of changes caused by the time of collection, or by underlying reduced activity levels in the mice, thus reducing CTX-II release from damaged cartilage. The mice were too far post-operatively to see the initial increase in serum CTX-II and the mice were too old to see elevation in urinary CTX-II. Collectively, our data indicates that while DMM+SD and DMM mice both developed OA, DMM+SD mice did not have exacerbated OA as we expected.

The pattern noted in the OA measures were similarly seen in the gastrointestinal tract evaluation; namely, in the ileum. F4/80+ expression in the ileum of DMM+SD mice was trending towards a significant decrease compared to DMM. Sections from the colon did not show differences in F4/80+ macrophage infiltration across any groups. There was a trend towards increased inflammation in both DMM and DMM+SD compared to Sham mice in the jejunum (Figure 9). Although our data do not show distinct differences across groups, we aimed to assess levels of inflammation in the ileum, jejunum, and colon because there are increasingly more studies about the connection of gastrointestinal health to systemic health and psychologic health. Studies addressing post-weaning stress of pigs have proven that regulatory systems of stress can communicate directly with the gastrointestinal tract. The HPA axis does this through CRF and its receptors present in the jejunum, ileum, and colon. As this system is activated, there is activation of inflammatory cells within the GI tract and subsequent damage to the tissues (Moeser, Pohl, & Rajput, 2017).

After evaluation of the GI tract inflammation and development of OA, the next set of data considered were cytokines. They were measured to evaluate overall systemic inflammation. Normalization methods were employed in hopes to minimize variation in values due to the mouse's size, kidney function, or polydipsia status. Since DMM+SD mice had lower bodyweight (Figure 1) and were polydipsic (data not shown), we wanted to ensure these factors did not falsely alter cytokines that could be excreted in the urine. It is also important to note that the Renin-Angiotensin-Aldosterone System (RAAS), a key component of blood pressure regulation and renal perfusion, may be affected by stress or depression components of this study. As angiotensin II is created within the pathway, aldosterone is released from the adrenal glands. Elevated aldosterone has been related to depression disorders and subsequent high blood pressure. This leads to a retention of fluid and electrolytes, and a subsequent alteration in renal function (Murck, Schussler, & Steiger, 2012).

Although our data suggests urinary clearance of cytokines or kidney function may influence serum concentrations, the literature has not yet established any consensus on appropriate normalization methods for biomarkers. Our data suggests, however, that renal excretion could be an important reason for the difficulty in finding biomarkers for many diseases, including OA. We did not have a direct measurement of creatinine clearance due to study limitations (urine output/24 hours was not an outcome measure) (Rodrigues et al., 2014). For this reason, the remainder of the discussion will only address the seven cytokines that showed significant differences in their serum concentration in order to draw more comparable conclusions with the existing literature (Figure 2). The cytokines in question are largely known for their involvement in innate immunity. IL-1β, IL-4, IL-6 IL-10, and TNFα levels are most commonly measured in mouse OA studies due to their additional importance in OA and roles in cartilage metabolism. IL-6 is generally anti-inflammatory in OA and promotes matrix metalloproteinase inhibitors (Caron, 2003; Lewis et al., 2011). G-CSF levels from mouse serum are elevated in inflammatory arthritis (Eyles et al., 2008). Another study, by Singh et al measured cytokines in human serum post-total knee arthroplasty before and after an injection (onabotulinum toxin A) as pain management. Eotaxin was elevated in this study, and was related to patients who reported less pain post-operatively (Singh, Noorbaloochi, & Knutson, 2017).

Most of the cytokines we saw alterations in are related through the innate immune response by eosinophils, basophils, and neutrophils, there is a possibility that the systemic response

observed in the present study was related solely to innate immunity. The cytokines that were specifically elevated here are more closely associated with eosinophils, basophils, and mast cells. However, eosinophils, basophils and mast cells have not been evaluated in OA to the best of our knowledge. Mast cells are a critical component of the gastrointestinal-brain-stress axis (Moeser et al., 2017). Evaluated cytokines could link all three components of this study through the monocyte-macrophage arm of the innate immune system. Monocytes, the precursors to macrophages, have been linked to social stress through activation of the β-adrenergic signaling pathway. One study looking at this particular pathway noted that social stress induces higher bone marrow output of monocytes, and this was blocked by β-adrenoreceptor antagonists. In other words, inhibition of the sympathetic nervous system, which is responsible for the traditional fight-or-flight response, corrected monocyte upregulation in chronic social defeat mice (Powell et al., 2013). Another study counter-intuitively linked increased corticosterone levels to increased release of monocytes from bone marrow through the CXCL12 cytokine during repeated social defeat encounters. Findings from Niraula et al study were different from the β-adrenergic study because corticosterone is related to the HPA axis regulatory body of stress (Niraula et al., 2018). Thus, the OA response to chronic stress could be a function of imbalance between the sympathetic-adrenal-medullary system and the HPA axis.

Down-stream activation of monocytes induces differentiation into macrophages. Activated macrophages have been explored in both systemic and localized immune response. These cells are simplistically divided into M1 or M2 classification. Generally speaking, the two macrophage groups are divided into “pathogen-killing” or “pro-inflammatory” M1 macrophages and “anti-inflammatory” M2 macrophages. M2 macrophages, however, have a heterogeneous function and can also be involved in pro-inflammatory processes (Roszer, 2015).

Importantly, activated macrophages have been studied in gastrointestinal homeostasis as well as musculoskeletal diseases. Activated gastrointestinal macrophages are largely local in nature, being present in multiple sections of the GI tract. Lamina propria, gut-associated lymphoid tissue, and Peyer’s patches each have a population of macrophages designed to clear pathogens that enter the body (Steinbach & Plevy, 2014). When GI tract homeostasis is altered, however, communication and mobilization of systemic cytokines can occur through the liver (de Jong, Gonzalez-Navajas, & Jansen, 2016). Therefore, if the combination of chronic stress and OA

interrupted gastrointestinal homeostasis of DMM and DMM+SD mice we would expect to see increased macrophages in the gastrointestinal tract.

Pro-inflammatory M1 activated macrophages within bone marrow from fractured mice femurs were correlated with eotaxin expression. Elevated levels of G-CSF, IL-6 and CXCL1 (KC) expression were likely associated with activation of dendritic cells. Dendritic cells may also be considered activated macrophages, but are tissue-resident specific. M1 cells were correlated with eotaxin, but M2 cells were not associated with any of the measured cytokines (McCauley, Bitsaktsis, & Cottrell, 2020). For the current study, this may suggest the systemic inflammatory process noted in DMM and DMM+SD mice is driven by communication between systemic inflammation and M1 macrophages or dendritic cell signaling from the joint, supporting the connection between OA and systemic health. In an inflammatory OA study, both acute phase and chronic phase inflammatory responses were considered. They found IL-6 was related to the acute phase of the inflammatory response. The group furthered the analysis and was able to relate this elevation to a rise in macrophage activation from the joint itself (Simon et al., 2001). Additional experiments would need to be performed for the present study to confirm the notion that the OA phenotype was driven by activated M1 macrophages or dendritic cells in the joint, but the Simon study was able to relate circulating cytokines to joint inflammation, further supporting the relation between local OA inflammation and systemic inflammation.

Although these findings explain why each measure may be altered in the context of each inflammatory process, they still do not explain why DMM+SD mice consistently have lower or similar results compared to DMM despite data showing they were more stressed during neurobehavioral analysis (data not shown) and had elevated levels of serum corticosterone (Figure 4). There are several possible explanations: increased serum corticosterone induced immunosuppression, reduced activity of the mice who were single housed for social isolation, or biological resilience (Dantzer, Cohen, Russo, & Dinan, 2018; Komori, 2015). Biologic resilience may occur when an individual adapts to cope with chronic stresses over prolonged periods of time. It is a difficult measure to assess since it is highly unique to each individual. Mallei et al, describes this phenomenon by measuring BDNF expression from hippocampus and pre-frontal cortex tissue. Their findings were different than normal chronic social defeat models because their mice experienced no changes in BDNF expression compared to control mice. Typical neurobiology studies show that chronic stress lowers BDNF expression in the brain (Mallei et al., 2019).

Although our results cannot be directly related to this study because we observed serum levels of BDNF and not brain levels of BDNF, it is interesting to note the correlation for future studies. Additionally, studies have shown that levels of IL-6 are lower in animals that show resilience to infectious agents (Dantzer et al., 2018). Our data showed that IL-6 in DMM+SD mice was decreased. Very few studies observe resilience with more than one cytokine observed, but our results are promising. Due to the limited number of studies addressing this issue, the topic obviously requires additional attention.

Limitations in the study were primarily due to unexpected variance in DMM+SD group. Additional outcome measures would help support or refute the current proposed mechanism. Additional bone parameters such as trabecular thickness, and cortical moments would strengthen arguments for patterns seen with OA. Comparing systemic cytokines to synovial fluid cytokines would help bridge the gap between systemic and local inflammation. Since the present study only observed F4/80+ macrophages in both gut and knees, specific macrophage markers could be employed to further explore the role of activated macrophages in OA and comorbidities. Other cell populations, for example, mast cells, could also be explored with markers such as mast cell tryptase. In summary, the present study showed that DMM+SD and DMM mice successfully OA, but that DMM+SD demonstrated a unique OA phenotype. Systemic inflammation, however, was less pronounced in DMM and DMM+SD than expected. Together the data confirm that multiple functional outcome measures are required to adequately describe the OA phenotype in animal models, and may be critical in evaluating novel therapeutic targets.

CHAPTER 4. MECHANOSENSITIVE CHANNELS AND OSTEOARTHRITIS

4.1 Mechanosensitive Channels and Osteoarthritis Methods

4.1.1 *Tissue Collection*

Tissues from fifteen cadaveric horses were collected within eight hours of euthanasia. All horses were euthanized for reasons other than lameness. Clinical history and pathologic findings were used to identify experimental groups: 1) no history of lameness or evidence of OA (n=11), 2) history of lameness or evidence of OA localized to fetlock joint (n=2), and 3) history of lameness localized to another joint, or evidence of OA localized to another joint (n=2). Paired forelimb dorsal fetlock joint capsule (DFC) and palmar fetlock joint capsule (PFC) were collected from all cases. If both limbs were not available, left limb tissues were collected. Additional joint capsule samples were also collected based on history of lameness, if indicated. In one case, a history of hind limb lameness was reported in the right stifle, however, necropsy findings did not report any gross changes in that joint so only forelimb samples were taken.

Joint capsule tissues were divided into immunohistochemistry wells and frozen at -80^{o}C embedded in Optimal Cutting Temperature (OTC) gel. Additional tissues were collected, minced, and washed in 10% Penicillin/Streptomycin/Amphotericin B (Pen/Strep/Fungizone) in Iscove's Modified Dulbecco's Medium (IMDM) before cell isolation.

4.1.2 *Cell Isolation and Culture*

Cell isolation was performed using a 0.2% collagenase-0.1% hyaluronidase digestion. After tissue collection, all tissues were minced and washed with 10% Pen/Strep/Fungizone in IMDM. A one-hour trypsin digestion (0.05% trypsin-EDTA in 1X PBS) was completed in a 37^{o}C oven prior to additional washes. The 0.2% collagenase-0.1% hyaluronidase digestion was performed in a 37^{o}C oven overnight. The resulting mixture was filtered using a 70 μm sterile cell filter before additional washes with ACK Lysing Buffer and isolation media (IMDM, Pen/Strep/Fungizone, and sodium pyruvate solution). Cells were counted with a Countess II Automated Cell Counter (Invitrogen Co., Carlsbad, CA, USA) and assessed for viability. Any cells

that were not immediately used for culture were frozen in custom freeze media (80% Fetal Bovine Serum, 10% DMEM-F12, and 10% DMSO) in liquid nitrogen.

Isolated cells were cultured in 25 cm^2 culture flasks at a density of 100,000 cells/flask until reaching 80-90% confluency (10-14 days). Confluent cells were removed from the flask using 0.05% trypsin-EDTA and re-assessed for quantity and viability. Viable cells were re-suspended in a custom media using 10% Multi-Species KnockOut Serum Replacement (10% SR Media) (Thermo Fisher Scientific, Waltham, MA, USA) before seeding into collagen gels.

4.1.3 *Immunohistochemistry*

DFC and PFC capsule samples frozen in OCT immediately after sample collection were sectioned using a Leica Biosystems Cryostat (Leica Biosystems Division of Leica Microsystems Inc., Buffalo Grove, IL, USA) at -20^{o}C. Four micrometer sections were collected using a specialized Cryo-film developed and described by Kawamoto (Section-Lab Co. Ltd., Yokohama, Kanagawa, Japan) (Kawamoto, 2003). Sections were fixed in 100% ethanol followed by 4% paraformaldehyde prior to staining on the Cryo-film. A horse-radish peroxidase immunohistochemistry kit (Abcam, Cambridge, United Kingdom) was used with Modified Mayer's hematoxylin for staining according to manufacturer protocols. Primary antibodies were selected for equine selectivity where possible. If untested previously, primary antibodies were selected for greatest homology and/or widest range of species suspected to work. See Appendix Table B1 for a list of primary antibodies and manufacturers selected. All samples were decolorized with distilled water baths and 100% ethanol prior to using Kawamoto mounting medium (SCMM-R2) and polymerizing using UV light.

All images were taken using an Olympus BX53 upright microscope with Olympus CellSens Dimensions software. Thresholds were determined using the CellSens Count and Measure add-on (Olympus Corporation, Shinjuku City, Tokyo, Japan). A ROI 500 μm along the synovial membrane by 100 μm deep was selected using measurement tools for imaging.

4.1.4 *Collagen Gel Contraction Assay*

Fibroblasts isolated through the 0.2% collagenase-0.1% hyaluronidase digestion were seeded into 5mg/mL bovine collagen type I gels (PureCol ® EZ Gel, Advanced BioMatrix,

Carlsbad, CA, USA). Cells were seeded at a density of 125,000 cells/well (250,000 cells/mL). Collagen gels were mixed and allowed to form according to manufacturer recommendations. Collagen gels were maintained in 24-well plates and incubated at 37^{o}C and 5% CO_2 for twelve hours before releasing the gels. 10% SR Media was used in conjunction with known agonists or antagonists towards mechanosensitive channels at serial concentrations. See Appendix Table B2 for agonists and antagonists used, and manufacturers.

After release, images were taken using a Nikon D3300 camera every 24 hours until there was evidence of collagen gel contraction. Once contraction started, images were taken every eight to twelve hours. Gels were imaged until contraction of the gels completed or contraction plateaued for more than two weeks post-release. Images were then loaded into ImageJ (National Institutes of Health, Bethesda, MD, USA) for measurements. The elliptical tool was used to circle the gel, and the resulting diameter was measured using a ruler included in the picture. Percent contraction was calculated based on measurements obtained from pictures at time of gel release (t=0 hrs) and plotted as a function of time.

4.2 Mechanosensitive Channels and Osteoarthritis Results

4.2.1 *Mechanosensitive Channel Immunohistochemistry*

Mechanosensitive channels have not been previously described in equine musculoskeletal soft tissues. All TRP and Piezo channel primary antibodies required extensive troubleshooting for positive control tissues as well as identifying appropriate dilutions for staining. TRPA1, TRPV1, TRPV4, and Piezo1 were first identified in tissues other than musculoskeletal soft tissue. TRPA1 and Piezo1 were both successfully identified in equine artery, while TRPV1 and TRPV4 were found in peripheral nerve and kidney, respectively.

After identifying in positive control tissues, staining was performed on experimental tissues (n=1; remainder delayed by COVID-19) from an otherwise healthy horse with no history of lameness. Figure 22 shows representative images from these results, including positive control tissues. These results were also used to develop appropriate thresholds in the CellSens Dimensions Count and Measure add-on, but the thresholds have not been applied to tissues for data collection, to date.

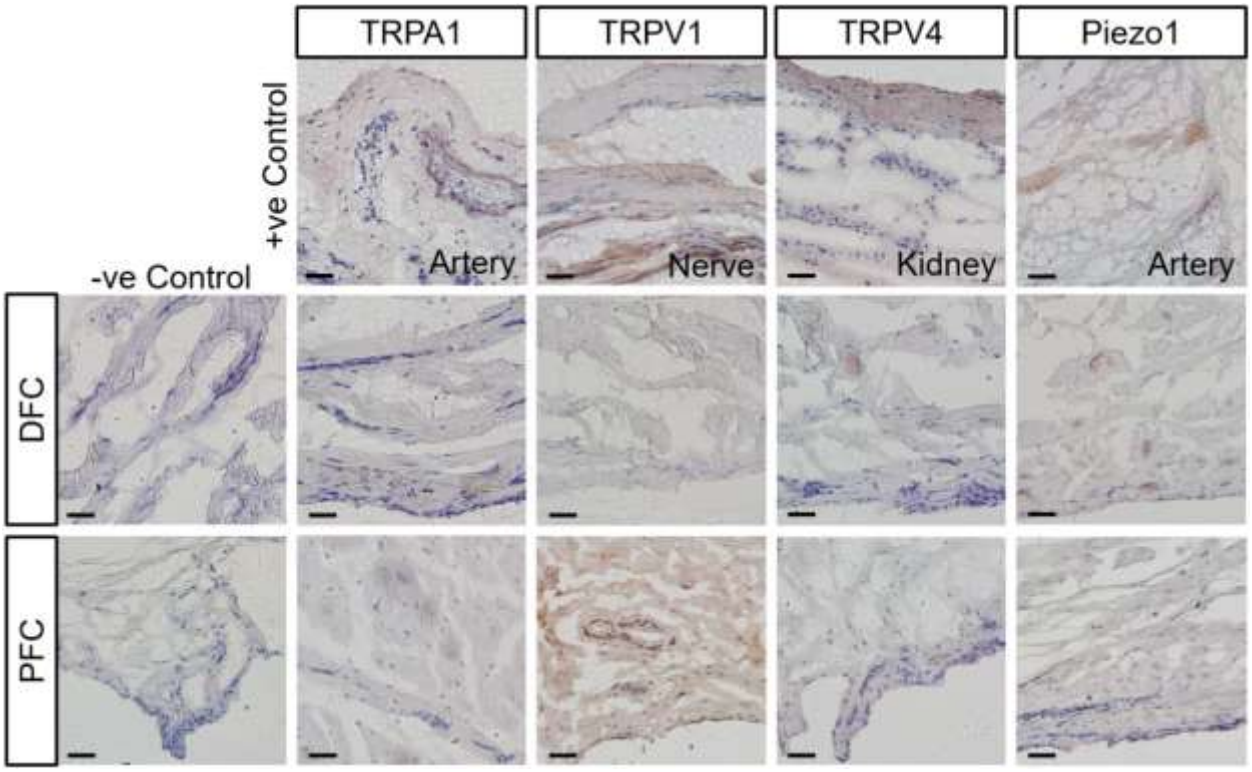

Figure 21. Representative Dorsal Fetlock Joint Capsule (DFC) sections and Palmar Fetlock Joint Capsule (PFC) sections with positive staining for TRPA1, TRPV1, TRPV4, and Piezo1 with corresponding positive (+ve) and negative (-ve) control tissues; Bar = 50 μm.

4.2.2 *Collagen Gel Contraction Assay*

To the best of our knowledge, fibroblasts from equine joint capsule tissue have not been previously used for collagen gel contraction assays. Initial attempts at seeding isolated fibroblasts from frozen aliquots into collagen gels were not successful. Adding a culture period before seeding and increasing the SR media from 1% to 10% seemed to help with these results.

The most recent gel was seeded with DFC fibroblast cells isolated from an otherwise healthy horse at 125,000 cells/well after a 10 day culture period. The cells were at 80% confluency before trypsinizing the culture and resuspending in collagen gel. Gels were maintained with serial concentrations (20 μM, 15 μM, 12 μM, 10 μM, and 5 μM) of amiloride hydrochloride, a non-specific ASIC channel antagonist. One well was maintained with no antagonist, but the same total volume of 10% SR Media. Another well was maintained with only amiloride hydrochloride vehicle (distilled water). The well that contained 5 μM amiloride hydrochloride was the first, and only well to contract thus far (delayed due to COVID-19). It began contracting within 24 hours post-release of the gel. The gel continued to contract over several days until most recent images

showed a pinpoint gel having a 0.03 cm^2 area compared to an initial 1.22 cm^2 area. Figure 23a shows the graph representing the percent contraction of all wells, while Figure 23b shows panels of representative images from the 5 μM well.

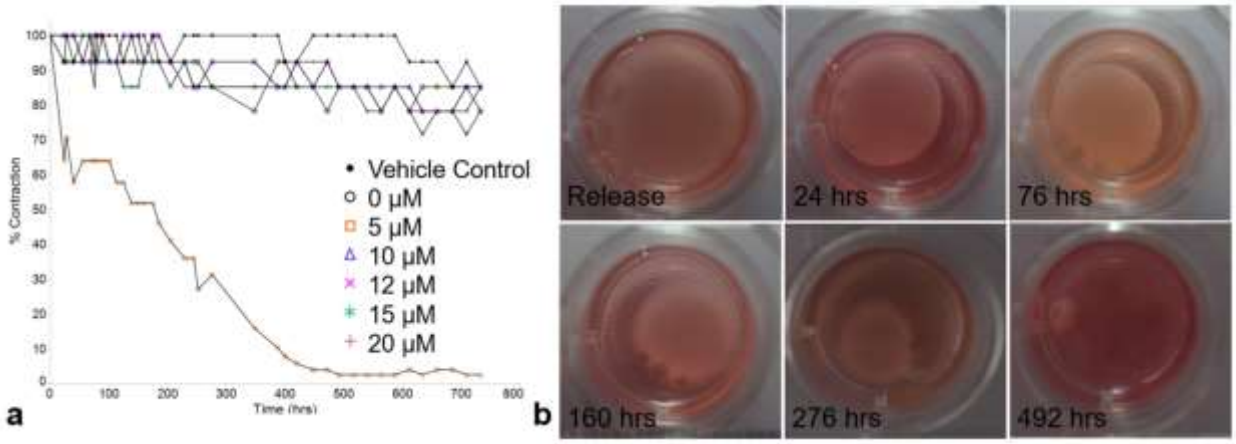

Figure 22. Collagen gel contraction assay; a) Percent contraction of gels over time; b) Representative images at specified time points for [Amiloride hydrochloride] = 5 μM.

4.3 Mechanosensitive Channels and Osteoarthritis Discussion

The second aim of this thesis attempted to show TRP and Piezo channel expression in equine joint capsule tissue from patients that had varying degrees of fetlock OA. We also attempted to characterize channel function in joint capsule fibroblasts from the same horses. Overall, we were able to show that equine joint capsule expresses mechanosensitive channels and normal fibroblasts will contract collagen gels variably with mechanosensitive channel blockade. We also collected enough tissues to further evaluate these measures in the future.

Previously, mechanosensitive channels including TRPA1, TRPV1, TRPV4, Peizo1, and Piezo2 have not been studied in equine tissues. Specifically, there were no reported studies showing expression of these channels in equine joint capsule. Positive control tissues such as artery, kidney, and peripheral nerve were found to have positive staining when compared to a negative control of the same tissue. Artery had positive staining for both TRPA1 and Piezo1 while peripheral nerve and kidney had positive staining for TRPV1 and TRPV4, respectively (Table B1). Control tissues were tested according to manufacturer recommendation, and alongside studies that have shown channel expression in other species (Alcaino et al., 2017; Andrei et al., 2017; Hyman et al., 2017; Xing & Li, 2017). Other positive control tissues that were attempted, but not successful, included jejunum and skin. These tissues were also used to determine working concentrations of

primary antibody for experimental tissue staining (Appendix Table B1). Because concentration of primary antibody for Piezo2 was not successfully found with positive control tissue, this antibody was excluded from staining on experimental tissues thus far.

DFC and PFC from a healthy horse were stained with primary antibody against TRPA1, TRPV1, TRPV4, and Piezo2. Both tissues were positive for all four channels, indicating that these channels are present in a normal horse without OA. It is also notable that there were different levels of expression when considering each channel in DFC or PFC. TRPV1 had the most notable difference where PFC had drastically more expression compared to DFC (Figure 22). Although definitive conclusions cannot be made with only one sample, the result is promising. PFC undergoes significantly more stretch during a horse's stride compared to the dorsal side (Butcher & Ashley-Ross, 2002). Asymmetric dorsal-palmar TRPV1 expression could eventually improve understanding of joint capsule injury and fetlock OA in horses.

In the collagen gel contraction assay, isolated fibroblasts were seeded at a density of 125,000 cells/well in a 24 well plate. Previous trials (results not shown) did not have successful contraction, likely due to difficulty in using previously frozen cells immediately after thaw for assays. Amiloride hydrochloride is a general antagonist that blocks ASICs. A previous study showed that amiloride hydrochloride was successful in blocking these channels at concentrations around 15 μM depending on tissue (Yu et al., 2015). The overall goal of including an ASIC channel antagonist will be more apparent when a complete set of assays are collected. Fibroblasts from each tissue location will be tested with various general antagonists, as well as, several agonists and antagonists that specifically target individual channels (e.g. E-capcaisin is a TRPV4 agonist and GSK 2193874 is a TRPV4 antagonist). Since TRP, Piezo and ASIC channels all have the potential to respond to inflammatory mediators, comparing results from several trials will help us narrow down which channels are playing a role in the fibroblasts' capability to contract a collagen gel. A total list of agonists and antagonists that will be tested are listed in Appendix Table B2.

It is unknown, to date, why the remaining wells did not begin contracting until day 19, and only contracted a small amount. Possibilities at this point include variable cell numbers in each well, permeability of media through the collagen gel, or contractility capabilities of normal fibroblasts after seeding. Since the well that contracted had 5 μM amiloride hydrochloride present, it is possible that ASIC antagonism could play a role in increasing the contractility capabilities of normal fibroblasts. However, similar concentrations of amiloride hydrochloride may also have

cross reactivity for blocking sodium-proton exchangers in rat fibroblasts (Santos-Torres, Slimak, Auer, & Ibanez-Tallon, 2011). Although we did not sort cells by flow cytometry, it is unlikely that the resulting isolated cells from the current protocol are not solely fibroblasts. Our protocol accounts for lysing red blood cells, and after monolayer expansion and several days in 3D culture, any residual white blood cells are unlikely to either initiate failure of gel contracture or be the major cell source that fails to contract. On the other hand, cells isolated from injured equine fetlock joint capsule may contain more myofibroblasts, and consequently express different or increased levels of mechanosensitive ion channels, as was identified in the anterior joint capsule of humans with shoulder OA (Chainani et al., 2020). Further, myofibroblasts are known for their contractility, and have been identified in both human and animal joint capsule after contracture injury (Hildebrand, Zhang, & Hart, 2007).

Although our initial amiloride hydrochloride trial raises more questions than answers, we can conclude that the fibroblasts isolated from equine joint capsule are still alive and functional at day 19 of culture. It is worth continuing with additional agonists and antagonists to observe additional contractility capabilities. Major limitations in this study were due to time constraints. The fact that both experiments had never been performed in the equine species, initial troubleshooting was largely unsuccessful, then COVID-19 restrictions limited progress after trouble-shooting was complete.

CHAPTER 5. SUMMARY AND CONCLUSIONS

In summary, this thesis had multiple findings when observing OA in the face of social stress. We found that chronic social defeat episodes do not necessarily exacerbate OA or measurements of systemic inflammation in single housed mice. On the contrary, combined chronic social defeat and PTOA may influence biologic resilience. The lack of changes between DMM and DMM+SD mice could also be explained by other mechanisms related to altered gait patterns or decreased movement in DMM+SD mice, or by the immunosuppressive effects of systemic increases in corticosterone. When comparing DMM and DMM+SD mice, cytokine patterns could reflect a mechanism connecting systemic health, stress, gastrointestinal health, and OA through the innate immune system and possibly macrophage activation.

The second study showed us that TRP and Piezo channels are expressed in normal equine DFC and PFC tissues. ASICs inhibition may paradoxically increase normal joint capsule fibroblast contraction capabilities. Although the results of the equine study could not definitively determine channel expression or influence of channels on fibroblast contraction of collagen gels, successful trials will focus future experiments on obtaining additional data. Furthermore, the proposed mechanism of activated macrophage involvement that was described by the social defeat study may also have a role within the mechanosensitive channel study. Previous studies have shown that TRP channels are largely involved in monocyte/macrophage functions, including polarization and in macrophage mediated transformation of fibroblasts to myofibroblasts (Santoni et al., 2018; Thodeti, Paruchuri, & Meszaros, 2013). This fact could be better explored through additional experiments for the second aim. Namely, fluorescence immunohistochemistry may be performed to identify co-expression of mechanosensitive channels and activated macrophages.

Ultimately, the overarching goal of this research would be to reflect both studies as they pertain to humans. Although additional studies should be done to address lingering questions in the case of both studies, the results of this thesis show promise for better explaining human OA. Through these two studies we were able to propose possible connections between OA and systemic health including systemic inflammation, gastrointestinal health, and stress. We would like to further this research to help explain why certain populations, such as LSES populations, have a higher incidence of OA. Connecting the results of the chronic social stress study to the equine

study would also help us understand how occupational overuse injuries may contribute to OA development and possibly how to target specific channels as a preventative measure.

APPENDIX A. CHRONIC SOCIAL STRESS AND OSTEOARTHRITIS SUPPLEMENTAL INFORMATION

Table A1. Average serum cytokine values by group and normalization method.

	Concentration			Body Weight Normalized			U Creat:S Creat Normalized			(U Creat:S Creat)/BSA Normalized		
	Sham	DMM	DMM+SD	Sham	DMM	DMM+SD	Sham	DMM	DMM+SD	Sham	DMM	DMM+SD
Eotaxin	2.93E+02	3.25E+02	3.28E+02	9.22E+00	1.01E+01	1.10E+01	2.88E-01	4.26E-01	3.43E-01	2.71E-01	4.01E-01	3.14E-01
G-CSF	1.67E+02	1.56E+02	2.34E+02	5.05E+00	4.75E+00	8.27E+00	1.61E-01	2.06E-01	2.58E-01	1.51E-01	1.96E-01	2.36E-01
GM-CSF	2.43E+00	1.58E+00	1.45E+00	7.98E-02	4.88E-02	4.87E-02	2.38E-03	2.07E-03	1.51E-03	2.25E-03	1.95E-03	1.38E-03
IFNy	2.45E-01	4.57E-01	5.04E-01	7.59E-03	1.47E-02	1.28E-02	2.43E-04	6.37E-04	4.04E-04	2.32E-04	5.84E-04	3.72E-04
IL-1a	3.55E+02	2.82E+02	2.86E+02	1.15E+01	8.63E+00	1.03E+01	3.70E-01	3.60E-01	3.16E-01	3.48E-01	3.41E-01	2.91E-01
IL-1B	1.63E+00	6.30E-01	2.27E+00	4.95E-02	1.95E-02	8.02E-02	2.16E-03	8.29E-04	2.39E-03	2.12E-03	7.82E-04	2.20E-03
IL-2	2.38E+00	1.86E+00	2.40E+00	6.79E-02	5.89E-02	6.93E-02	2.07E-03	2.42E-03	2.19E-03	1.97E-03	2.25E-03	1.99E-03
IL-3	3.81E-01	6.33E-01	7.92E-02	1.33E-02	1.97E-02	2.68E-03	3.71E-04	8.03E-04	8.30E-05	3.51E-04	7.44E-04	7.60E-05
IL-4	4.00E-02	7.23E-01	1.28E-01	1.34E-03	2.26E-02	4.54E-03	4.20E-05	8.78E-04	1.35E-04	4.00E-05	8.06E-04	1.24E-04
IL-5	4.51E+00	5.29E+00	2.52E+00	1.32E-01	1.64E-01	8.33E-02	4.25E-03	6.76E-03	2.52E-03	3.99E-03	6.35E-03	2.30E-03
IL-6	7.63E-01	2.08E+00	4.32E-01	2.40E-02	6.47E-02	1.38E-02	7.90E-04	2.57E-03	4.48E-04	7.52E-04	2.38E-03	4.06E-04
IL-7	1.53E+00	7.37E+01	7.12E-01	3.26E-02	2.19E+00	2.45E-02	1.11E-03	8.97E-02	7.83E-04	1.06E-03	8.54E-02	7.14E-04
IL-9	4.88E+01	4.07E+01	4.64E+01	1.66E+00	1.25E+00	1.52E+00	5.19E-02	5.44E-02	4.73E-02	4.88E-02	5.14E-02	4.33E-02
IL-10	1.52E+00	2.19E+01	1.65E+00	5.01E-02	6.86E-01	5.82E-02	1.44E-03	2.66E-02	1.74E-03	1.37E-03	2.44E-02	1.59E-03
IL-12 (p40)	2.15E+01	6.22E+00	3.81E+00	7.26E-01	1.94E-01	1.25E-01	2.04E-02	8.11E-03	3.88E-03	1.94E-02	7.61E-03	3.53E-03
IL-12 (p70)	8.12E+00	4.12E+01	9.93E+00	2.74E-01	1.29E+00	3.45E-01	8.56E-03	5.06E-02	1.04E-02	8.13E-03	4.66E-02	9.51E-03
IL-13	1.02E+01	9.85E+00	8.04E+00	3.26E-01	3.05E-01	2.59E-01	1.01E-02	1.31E-02	8.04E-03	9.53E-03	1.23E-02	7.34E-03
IL-15	1.25E+01	7.18E+02	8.98E+00	2.88E-01	2.13E+01	3.04E-01	9.00E-03	8.66E-01	9.22E-03	8.45E-03	8.25E-01	8.31E-03
IL-17	7.46E-01	1.20E+00	9.52E-01	2.43E-02	3.78E-02	3.16E-02	7.59E-04	1.57E-03	9.86E-04	7.11E-04	1.47E-03	9.02E-04
IP-10	3.13E+01	3.10E+01	2.58E+01	9.75E-01	9.63E-01	8.34E-01	3.12E-02	4.10E-02	2.62E-02	2.95E-02	3.85E-02	2.40E-02
KC	8.68E+01	1.08E+02	6.96E+01	2.75E+00	3.34E+00	2.25E+00	8.55E-02	1.42E-01	6.98E-02	8.05E-02	1.34E-01	6.38E-02
LIF	5.00E-01	6.72E+00	1.07E+00	1.50E-02	1.99E-01	3.82E-02	5.35E-04	8.13E-03	1.27E-03	5.14E-04	7.74E-03	1.16E-03
LIX	4.22E+03	4.13E+03	4.58E+03	1.25E+02	1.27E+02	1.61E+02	3.95E+00	5.34E+00	4.99E+00	3.72E+00	5.06E+00	4.57E+00
MCP-1	1.09E+01	1.11E+01	1.32E+01	3.45E-01	3.38E-01	4.47E-01	1.09E-02	1.42E-02	1.33E-02	1.04E-02	1.34E-02	1.22E-02
M-CSF	2.84E+01	2.67E+00	7.21E+00	9.58E-01	8.32E-02	2.54E-01	2.81E-02	3.55E-03	8.15E-03	2.69E-02	3.33E-03	7.37E-03
MIG	6.34E+00	2.34E+01	6.16E+00	2.03E-01	7.00E-01	2.08E-01	6.45E-03	2.87E-02	6.44E-03	6.13E-03	2.73E-02	5.90E-03
MIP-1a	1.97E+01	1.93E+01	1.99E+01	6.58E-01	6.02E-01	6.84E-01	2.01E-02	2.61E-02	2.14E-02	1.90E-02	2.45E-02	1.96E-02
MIP-1B	1.13E+01	1.41E+01	8.43E+00	3.28E-01	4.40E-01	2.90E-01	9.99E-03	1.87E-02	9.19E-03	9.50E-03	1.75E-02	8.51E-03
MIP-2	5.65E+01	4.37E+01	4.60E+01	1.92E+00	1.36E+00	1.44E+00	5.44E-02	5.90E-02	4.48E-02	5.09E-02	5.55E-02	4.12E-02
RANTES	1.84E+01	1.61E+01	1.63E+01	5.56E-01	5.10E-01	5.33E-01	1.65E-02	2.08E-02	1.74E-02	1.56E-02	1.93E-02	1.61E-02
TNFa	1.09E+00	9.12E-01	1.68E+00	3.88E-02	2.86E-02	5.69E-02	1.05E-03	1.26E-03	1.69E-03	9.88E-04	1.17E-03	1.54E-03
VEGF	5.29E-01	3.79E-01	4.04E-01	1.64E-02	1.18E-02	1.36E-02	5.26E-04	5.03E-04	4.27E-04	5.03E-04	4.73E-04	3.91E-04

APPENDIX B. MECHANOSENSITIVE CHANNELS AND OSTEOARTHRITIS SUPPLEMENTAL INFORMATION

Table B1. Positive control tissues, dilutions and manufacturers of primary antibodies used on equine joint capsule tissues.

Antibody	Positive Control Tissue	Dilution	Manufacturer
Anti-TRPA1	Artery	1:1000	Novus Biologicals, LLC
Anti-TRPV1	Peripheral Nerve	1:400	Novus Biologicals, LLC
Anti-TRPV4	Kidney	1:200	Abcam
Anti-Piezo1	Artery	1:100	Novus Biologicals, LLC
Anti-Piezo2	Undetermined	Undetermined	Novus Biologicals, LLC

Table B2. Calcium channel targets and manufacturers of agonists and antagonists used with equine joint capsule fibroblasts.

Calcium Channel Target	Compound	Agonist/Antagonist	Manufacturer
Non-Specific	Ruthenium Red	Antagonist	Sigma-Aldrich, Inc.
Mechanosensitive	Gadolinium Chloride	Antagonist	Sigma-Aldrich, Inc.
ASIC Non-Specific	Amiloride Hydrochloride	Antagonist	Sigma-Aldrich, Inc.
TRPV4	E-Capsaicin	Agonist	Sigma-Aldrich, Inc.
TRPM8, TRPA1	Icilin	Agonist	Sigma-Aldrich, Inc.
TRPV1	Ananadamide	Agonist	Sigma-Aldrich, Inc.
TRPV4	RN 1747	Agonist	Sigma-Aldrich, Inc.
TRPA1	ASP 7663	Agonist	Sigma-Aldrich, Inc.
TRPV	Capsazepine	Antagonist	Sigma-Aldrich, Inc.
TRPA1	HC 030031	Antagonist	Sigma-Aldrich, Inc.
TRPV1	AMG 21629	Antagonist	Tocris Bioscience
TRPV4	GSK 2193874	Antagonist	Tocris Bioscience
TRPC1, TRPC6, Piezo1, Piezo2	GsMTx4	Antagonist	Tocris Bioscience
Piezo1	Yoda1	Agonist	Sigma-Aldrich, Inc.

REFERENCES

Alcaino, C., Farrugia, G., & Beyder, A. (2017). Mechanosensitive Piezo Channels in the Gastrointestinal Tract. *Curr Top Membr, 79*, 219-244. doi:10.1016/bs.ctm.2016.11.003

Andrei, S. R., Ghosh, M., Sinharoy, P., Dey, S., Bratz, I. N., & Damron, D. S. (2017). TRPA1 ion channel stimulation enhances cardiomyocyte contractile function via a CaMKII-dependent pathway. *Channels (Austin), 11*(6), 587-603. doi:10.1080/19336950.2017.1365206

Arthur, R. M., Blea, J. A., Ross, M. W., Moloney, P. J., & Cheney, M. W. (2011). The North American Thoroughbred. In *Diagnosis and Management of Lameness in the Horse* (pp. 977-993).

Bathina, S., & Das, U. N. (2015). Brain-derived neurotrophic factor and its clinical implications. *Arch Med Sci, 11*(6), 1164-1178. doi:10.5114/aoms.2015.56342

Bertram, K. L., Banderali, U., Tailor, P., & Krawetz, R. J. (2016). Ion channel expression and function in normal and osteoarthritic human synovial fluid progenitor cells. *Channels (Austin), 10*(2), 148-157. doi:10.1080/19336950.2015.1116652

Bortoluzzi, A., Furini, F., & Scire, C. A. (2018). Osteoarthritis and its management - Epidemiology, nutritional aspects and environmental factors. *Autoimmun Rev, 17*(11), 1097-1104. doi:10.1016/j.autrev.2018.06.002

Buch, T. R. H., Buch, E. A. M., Boekhoff, I., Steinritz, D., & Aigner, A. (2018). Role of Chemosensory TRP Channels in Lung Cancer. *Pharmaceuticals (Basel), 11*(4). doi:10.3390/ph11040090

Butcher, M., & Ashley-Ross, M. (2002). Fetlock joint kinematics differ with age in thoroughbred racehorses. *Journal of Biomechanics, 35*, 563-571.

Cai, G., Otahal, P., Cicuttini, F., Wu, F., Munugoda, I. P., Jones, G., & Aitken, D. (2020). The association of subchondral and systemic bone mineral density with osteoarthritis-related joint replacements in older adults. *Osteoarthritis Cartilage, 28*(4), 438-445. doi:10.1016/j.joca.2020.02.832

Carballo, C. B., Hutchinson, I. D., Album, Z. M., Mosca, M. J., Hall, A., Rodeo, S., Jr., . . . Rodeo, S. A. (2018). Biomechanics and Microstructural Analysis of the Mouse Knee and Ligaments. *J Knee Surg, 31*(6), 520-527. doi:10.1055/s-0037-1604151

Caron, J. (2003). Osteoarthritis. In M. W. Ross (Ed.), *Diagnosis and Management of Lameness in the Horse*: Elsevier Inc.

Chainani, A., Matson, A., Chainani, M., Marchand Colon, A. J., Toth, A. P., Garrigues, G. E., & Little, D. (2020). Contracture and transient receptor potential channel upregulation in the anterior glenohumeral joint capsule of patients with end-stage osteoarthritis. *J Shoulder Elbow Surg*. doi:10.1016/j.jse.2019.11.013

Coste, B., Mathur, J., Schmidt, M., Earley, T. J., Ranade, S., Petrus, M. J., . . . Patapoutian, A. (2010). Piezo1 and Piezo2 are essential components of distinct mechanically activated cation channels. *Science, 330*(6000), 55-60. doi:10.1126/science.1193270

Cristofori-Armstrong, B., & Rash, L. D. (2017). Acid-sensing ion channel (ASIC) structure and function: Insights from spider, snake and sea anemone venoms. *Neuropharmacology, 127*, 173-184. doi:10.1016/j.neuropharm.2017.04.042

Cryan, J. F., & Holmes, A. (2005). The ascent of mouse: advances in modelling human depression and anxiety. *Nat Rev Drug Discov, 4*(9), 775-790. doi:10.1038/nrd1825

Dadomo, H., Sanghez, V., Di Cristo, L., Lori, A., Ceresini, G., Malinge, I., . . . Bartolomucci, A. (2011). Vulnerability to chronic subordination stress-induced depression-like disorders in adult 129SvEv male mice. *Prog Neuropsychopharmacol Biol Psychiatry, 35*(6), 1461-1471. doi:10.1016/j.pnpbp.2010.11.016

Dantzer, R., Cohen, S., Russo, S. J., & Dinan, T. G. (2018). Resilience and immunity. *Brain Behav Immun, 74*, 28-42. doi:10.1016/j.bbi.2018.08.010

de Jong, P. R., Gonzalez-Navajas, J. M., & Jansen, N. J. (2016). The digestive tract as the origin of systemic inflammation. *Crit Care, 20*(1), 279. doi:10.1186/s13054-016-1458-3

Decker, R. S. (2017). Articular cartilage and joint development from embryogenesis to adulthood. *Semin Cell Dev Biol, 62*, 50-56. doi:10.1016/j.semcdb.2016.10.005

Duclos, M. E., Roualdes, O., Cararo, R., Rousseau, J. C., Roger, T., & Hartmann, D. J. (2010). Significance of the serum CTX-II level in an osteoarthritis animal model: a 5-month longitudinal study. *Osteoarthritis Cartilage, 18*(11), 1467-1476. doi:10.1016/j.joca.2010.07.007

Eleswarapu, S. V., & Athanasiou, K. A. (2013). TRPV4 channel activation improves the tensile properties of self-assembled articular cartilage constructs. *Acta Biomater, 9*(3), 5554-5561. doi:10.1016/j.actbio.2012.10.031

Eyles, J. L., Hickey, M. J., Norman, M. U., Croker, B. A., Roberts, A. W., Drake, S. F., . . . Wicks, I. P. (2008). A key role for G-CSF-induced neutrophil production and trafficking during inflammatory arthritis. *Blood, 112*(13), 5193-5201. doi:10.1182/blood-2008-02-139535

Felson, D. T., Naimark, A., Anderson, J., Kazis, L., Castelli, W., & Meenan, R. (1987). The Prevalence of Knee Osteoarthritis in the Elderly. *Arthritis and Rheumatism, 30*(8).

Furman, B. D., Strand, J., Hembree, W. C., Ward, B. D., Guilak, F., & Olson, S. A. (2007). Joint degeneration following closed intraarticular fracture in the mouse knee: a model of posttraumatic arthritis. *J Orthop Res, 25*(5), 578-592. doi:10.1002/jor.20331

Gavenis, K., Schumacher, C., Schneider, U., Eisfeld, J., Mollenhauer, J., & Schmidt-Rohlfing, B. (2009). Expression of ion channels of the TRP family in articular chondrocytes from osteoarthritic patients: changes between native and in vitro propagated chondrocytes. *Mol Cell Biochem, 321*(1-2), 135-143. doi:10.1007/s11010-008-9927-x

Ge, J., Li, W., Zhao, Q., Li, N., Chen, M., Zhi, P., . . . Yang, M. (2015). Architecture of the mammalian mechanosensitive Piezo1 channel. *Nature, 527*(7576), 64-69. doi:10.1038/nature15247

Glasson, S. S., Blanchet, T. J., & Morris, E. A. (2007). The surgical destabilization of the medial meniscus (DMM) model of osteoarthritis in the 129/SvEv mouse. *Osteoarthritis Cartilage, 15*(9), 1061-1069. doi:10.1016/j.joca.2007.03.006

Golden, S. A., Covington, H. E., 3rd, Berton, O., & Russo, S. J. (2011). A standardized protocol for repeated social defeat stress in mice. *Nat Protoc, 6*(8), 1183-1191. doi:10.1038/nprot.2011.361

Goto, T., Kubota, Y., Tanaka, Y., Iio, W., Moriya, N., & Toyoda, A. (2014). Subchronic and mild social defeat stress accelerates food intake and body weight gain with polydipsia-like features in mice. *Behav Brain Res, 270*, 339-348. doi:10.1016/j.bbr.2014.05.040

Gregory, N. S., Harris, A. L., Robinson, C. R., Dougherty, P. M., Fuchs, P. N., & Sluka, K. A. (2013). An overview of animal models of pain: disease models and outcome measures. *J Pain, 14*(11), 1255-1269. doi:10.1016/j.jpain.2013.06.008

Guilak, F. (2011). Biomechanical factors in osteoarthritis. *Best Pract Res Clin Rheumatol, 25*(6), 815-823. doi:10.1016/j.berh.2011.11.013

Hantute-Ghesquier, A., Haustrate, A., Prevarskaya, N., & Lehen'kyi, V. (2018). TRPM Family Channels in Cancer. *Pharmaceuticals (Basel), 11*(2). doi:10.3390/ph11020058

Haraden, C. A., Huebner, J. L., Hsueh, M. F., Li, Y. J., & Kraus, V. B. (2019). Synovial fluid biomarkers associated with osteoarthritis severity reflect macrophage and neutrophil related inflammation. *Arthritis Res Ther, 21*(1), 146. doi:10.1186/s13075-019-1923-x

Hildebrand, K. A., Zhang, M., & Hart, D. A. (2007). Myofibroblast upregulators are elevated in joint capsules in posttraumatic contractures. *Clin Orthop Relat Res, 456*, 85-91. doi:10.1097/BLO.0b013e3180312c01

Hiligsmann, M., Cooper, C., Arden, N., Boers, M., Branco, J. C., Luisa Brandi, M., . . . Reginster, J. Y. (2013). Health economics in the field of osteoarthritis: an expert's consensus paper from the European Society for Clinical and Economic Aspects of Osteoporosis and Osteoarthritis (ESCEO). *Semin Arthritis Rheum, 43*(3), 303-313. doi:10.1016/j.semarthrit.2013.07.003

Hokamp, J. A., & Nabity, M. B. (2016). Renal biomarkers in domestic species. *Vet Clin Pathol, 45*(1), 28-56. doi:10.1111/vcp.12333

Hollis, F., & Kabbaj, M. (2014). Social defeat as an animal model for depression. *ILAR J, 55*(2), 221-232. doi:10.1093/ilar/ilu002

Holzer, P. (2015). Acid-sensing ion channels in gastrointestinal function. *Neuropharmacology, 94*, 72-79. doi:10.1016/j.neuropharm.2014.12.009

Hyman, A. J., Tumova, S., & Beech, D. J. (2017). Piezo1 Channels in Vascular Development and the Sensing of Shear Stress. *Curr Top Membr, 79*, 37-57. doi:10.1016/bs.ctm.2016.11.001

Iijima, H., Aoyama, T., Fukutani, N., Isho, T., Yamamoto, Y., Hiraoka, M., . . . Matsuda, S. (2018). Psychological health is associated with knee pain and physical function in patients with knee osteoarthritis: an exploratory cross-sectional study. *BMC Psychol, 6*(1), 19. doi:10.1186/s40359-018-0234-3

Itoh, Y., Hatano, N., Hayashi, H., Onozaki, K., Miyazawa, K., & Muraki, K. (2009). An environmental sensor, TRPV4 is a novel regulator of intracellular Ca2+ in human synoviocytes. *Am J Physiol Cell Physiol, 297*(5), C1082-1090. doi:10.1152/ajpcell.00204.2009

Kawamoto, T. (2003). Use of a new adhesive film for the preparation o multi-purpose fresh-frozen sections from hard tissues, whole animals, insects and plants. *Archives of Histology and Cytology, 66*(2), 123-143.

Khatib, Y., Jenkin, D., Naylor, J. M., & Harris, I. A. (2016). Psychological Traits in Patients Waiting for Total Knee Arthroplasty. A Cross-sectional Study. *J Arthroplasty, 31*(8), 1661-1666. doi:10.1016/j.arth.2016.01.053

Kobayashi, H., Yoshiyama, M., Zakoji, H., Takeda, M., & Araki, I. (2009). Sex differences in the expression profile of acid-sensing ion channels in the mouse urinary bladder: a possible involvement in irritative bladder symptoms. *BJU Int, 104*(11), 1746-1751. doi:10.1111/j.1464-410X.2009.08658.x

Komori, T. (2015). Animal models for osteoporosis. *Eur J Pharmacol, 759*, 287-294. doi:10.1016/j.ejphar.2015.03.028

Komori, T. (2016). Glucocorticoid Signaling and Bone Biology. *Horm Metab Res, 48*(11), 755-763. doi:10.1055/s-0042-110571

Korda, R., Paige, E., Yiengprugsawan, V., Latz, I., & Friel, S. (2014). Income-related inequalities in chronic conditions, physical functioning and psychologic distress among older people in Australia: cross-sectional findings from the 45 and up study. *BMC Public Health, 14*.

Krishnan, V., Han, M. H., Graham, D. L., Berton, O., Renthal, W., Russo, S. J., . . . Nestler, E. J. (2007). Molecular adaptations underlying susceptibility and resistance to social defeat in brain reward regions. *Cell, 131*(2), 391-404. doi:10.1016/j.cell.2007.09.018

Lee, W., Guilak, F., & Liedtke, W. (2017). Role of Piezo Channels in Joint Health and Injury. *Curr Top Membr, 79*, 263-273. doi:10.1016/bs.ctm.2016.10.003

Lee, W., Leddy, H. A., Chen, Y., Lee, S. H., Zelenski, N. A., McNulty, A. L., . . . Liedtke, W. B. (2014). Synergy between Piezo1 and Piezo2 channels confers high-strain mechanosensitivity to articular cartilage. *Proc Natl Acad Sci U S A, 111*(47), E5114-5122. doi:10.1073/pnas.1414298111

Lewis, J. S., Hembree, W. C., Furman, B. D., Tippets, L., Cattel, D., Huebner, J. L., . . . Olson, S. A. (2011). Acute joint pathology and synovial inflammation is associated with increased intra-articular fracture severity in the mouse knee. *Osteoarthritis Cartilage, 19*(7), 864-873. doi:10.1016/j.joca.2011.04.011

Lotteau, S., Ducreux, S., Romestaing, C., Legrand, C., & Van Coppenolle, F. (2013). Characterization of functional TRPV1 channels in the sarcoplasmic reticulum of mouse skeletal muscle. *PLoS One, 8*(3), e58673. doi:10.1371/journal.pone.0058673

Mallei, A., Ieraci, A., & Popoli, M. (2019). Chronic social defeat stress differentially regulates the expression of BDNF transcripts and epigenetic modifying enzymes in susceptible and resilient mice. *World J Biol Psychiatry, 20*(7), 555-566. doi:10.1080/15622975.2018.1500029

Martin, J. A., Anderson, D. D., Goetz, J. E., Fredericks, D., Pedersen, D. R., Ayati, B. P., . . . Buckwalter, J. A. (2017). Complementary models reveal cellular responses to contact stresses that contribute to post-traumatic osteoarthritis. *J Orthop Res, 35*(3), 515-523. doi:10.1002/jor.23389

McCauley, J., Bitsaktsis, C., & Cottrell, J. (2020). Macrophage subtype and cytokine expression characterization during the acute inflammatory phase of mouse bone fracture repair. *J Orthop Res*. doi:10.1002/jor.24603

McGowan, C. M., & Ireland, J. L. (2016). Welfare, Quality of Life, and Euthanasia of Aged Horses. *Vet Clin North Am Equine Pract, 32*(2), 355-367. doi:10.1016/j.cveq.2016.04.011

McQuaid, R. J., Audet, M. C., Jacobson-Pick, S., & Anisman, H. (2013). Environmental enrichment influences brain cytokine variations elicited by social defeat in mice. *Psychoneuroendocrinology, 38*(7), 987-996. doi:10.1016/j.psyneuen.2012.10.003

Minke, B. (2010). The history of the Drosophila TRP channel: the birth of a new channel superfamily. *J Neurogenet, 24*(4), 216-233. doi:10.3109/01677063.2010.514369

Moeser, A. J., Pohl, C. S., & Rajput, M. (2017). Weaning stress and gastrointestinal barrier development: Implications for lifelong gut health in pigs. *Anim Nutr, 3*(4), 313-321. doi:10.1016/j.aninu.2017.06.003

Murck, H., Schussler, P., & Steiger, A. (2012). Renin-angiotensin-aldosterone system: the forgotten stress hormone system: relationship to depression and sleep. *Pharmacopsychiatry, 45*(3), 83-95. doi:10.1055/s-0031-1291346

Neurobiology of TRP Channels. (2017). (T. Emir Ed. 2nd ed.). Boca Raton, FL: CRC Press/Taylor & Francis.

Newman, E. L., Covington, H. E., 3rd, Suh, J., Bicakci, M. B., Ressler, K. J., DeBold, J. F., & Miczek, K. A. (2019). Fighting Females: Neural and Behavioral Consequences of Social Defeat Stress in Female Mice. *Biol Psychiatry, 86*(9), 657-668. doi:10.1016/j.biopsych.2019.05.005

Nielsen, R. H., Stoop, R., Leeming, D. J., Stolina, M., Qvist, P., Christiansen, C., & Karsdal, M. A. (2008). Evaluation of cartilage damage by measuring collagen degradation products in joint extracts in a traumatic model of osteoarthritis. *Biomarkers, 13*(1), 79-87. doi:10.1080/13547500701615108

Niraula, A., Wang, Y., Godbout, J. P., & Sheridan, J. F. (2018). Corticosterone Production during Repeated Social Defeat Causes Monocyte Mobilization from the Bone Marrow, Glucocorticoid Resistance, and Neurovascular Adhesion Molecule Expression. *J Neurosci, 38*(9), 2328-2340. doi:10.1523/JNEUROSCI.2568-17.2018

Nummenmaa, E., Hamalainen, M., Moilanen, L. J., Paukkeri, E. L., Nieminen, R. M., Moilanen, T., . . . Moilanen, E. (2016). Transient receptor potential ankyrin 1 (TRPA1) is functionally expressed in primary human osteoarthritic chondrocytes. *Arthritis Res Ther, 18*(1), 185. doi:10.1186/s13075-016-1080-4

O'Conor, C. J., Leddy, H. A., Benefield, H. C., Liedtke, W. B., & Guilak, F. (2014). TRPV4-mediated mechanotransduction regulates the metabolic response of chondrocytes to dynamic loading. *Proc Natl Acad Sci U S A, 111*(4), 1316-1321. doi:10.1073/pnas.1319569111

O'Conor, C. J., Ramalingam, S., Zelenski, N. A., Benefield, H. C., Rigo, I., Little, D., . . . Guilak, F. (2016). Cartilage-Specific Knockout of the Mechanosensory Ion Channel TRPV4 Decreases Age-Related Osteoarthritis. *Sci Rep, 6*, 29053. doi:10.1038/srep29053

O'Neill, T. W., McCabe, P. S., & McBeth, J. (2018). Update on the epidemiology, risk factors and disease outcomes of osteoarthritis. *Best Pract Res Clin Rheumatol, 32*(2), 312-326. doi:10.1016/j.berh.2018.10.007

Olvera Alvarez, H. A., Kubzansky, L. D., Campen, M. J., & Slavich, G. M. (2018). Early life stress, air pollution, inflammation, and disease: An integrative review and immunologic model of social-environmental adversity and lifespan health. *Neurosci Biobehav Rev, 92*, 226-242. doi:10.1016/j.neubiorev.2018.06.002

Passini, F., Saab, A., Jaeger, P., Arlt, M., Ferrari, K., Haenni, D., . . . Snedeker, J. (2019). *PIEZO1 Senses Mechanical Loading and Induces Nanomolar Calcium Signals in Tendon Cells.* Paper presented at the Orthopaedic Research Society Annual Meeting, Austin, TX.

Pignataro, G., Cuomo, O., Esposito, E., Sirabella, R., Di Renzo, G., & Annunziato, L. (2011). ASIC1a contributes to neuroprotection elicited by ischemic preconditioning and postconditioning. *International Journal of Physiology, Pathophysiology and Pharmacology, 3*(1), 1-8.

Powell, N. D., Sloan, E. K., Bailey, M. T., Arevalo, J. M., Miller, G. E., Chen, E., . . . Cole, S. W. (2013). Social stress up-regulates inflammatory gene expression in the leukocyte transcriptome via beta-adrenergic induction of myelopoiesis. *Proc Natl Acad Sci U S A, 110*(41), 16574-16579. doi:10.1073/pnas.1310655110

Raubenheimer, P. J., Young, E. A., Andrew, R., & Seckl, J. R. (2006). The role of corticosterone in human hypothalamic-pituitary-adrenal axis feedback. *Clin Endocrinol (Oxf), 65*(1), 22-26. doi:10.1111/j.1365-2265.2006.02540.x

Razzoli, M., Carboni, L., Andreoli, M., Ballottari, A., & Arban, R. (2011). Different susceptibility to social defeat stress of BalbC and C57BL6/J mice. *Behav Brain Res, 216*(1), 100-108. doi:10.1016/j.bbr.2010.07.014

Reed, S. R., Jackson, B. F., Mc Ilwraith, C. W., Wright, I. M., Pilsworth, R., Knapp, S., . . . Verheyen, K. L. (2012). Descriptive epidemiology of joint injuries in Thoroughbred racehorses in training. *Equine Vet J, 44*(1), 13-19. doi:10.1111/j.2042-3306.2010.00352.x

Reyes, C., Garcia-Gil, M., Elorza, J. M., Mendez-Boo, L., Hermosilla, E., Javaid, M. K., . . . Prieto-Alhambra, D. (2015). Socio-economic status and the risk of developing hand, hip or knee osteoarthritis: a region-wide ecological study. *Osteoarthritis Cartilage, 23*(8), 1323-1329. doi:10.1016/j.joca.2015.03.020

Richardson, D. W., & Dyson, S. J. (2011). The Metacarpophalangeal Joint. In *Diagnosis and Management of Lameness in the Horse* (pp. 394-410).

Rodrigues, W. F., Miguel, C. B., Napimoga, M. H., Oliveira, C. J., & Lazo-Chica, J. E. (2014). Establishing standards for studying renal function in mice through measurements of body size-adjusted creatinine and urea levels. *Biomed Res Int, 2014*, 872827. doi:10.1155/2014/872827

Roszer, T. (2015). Understanding the Mysterious M2 Macrophage through Activation Markers and Effector Mechanisms. *Mediators Inflamm, 2015*, 816460. doi:10.1155/2015/816460

Santoni, G., Morelli, M. B., Amantini, C., Santoni, M., Nabissi, M., Marinelli, O., & Santoni, A. (2018). "Immuno-Transient Receptor Potential Ion Channels": The Role in Monocyte- and Macrophage-Mediated Inflammatory Responses. *Front Immunol, 9*, 1273. doi:10.3389/fimmu.2018.01273

Santos-Torres, J., Slimak, M. A., Auer, S., & Ibanez-Tallon, I. (2011). Cross-reactivity of acid-sensing ion channel and Na(+)-H(+) exchanger antagonists with nicotinic acetylcholine receptors. *J Physiol, 589*(Pt 21), 5109-5123. doi:10.1113/jphysiol.2011.213272

Sarukawa, J., Takahashi, M., Doi, M., Suzuki, D., & Nagano, A. (2010). A longitudinal analysis of urinary biochemical markers and bone mineral density in STR/Ort mice as a model of spontaneous osteoarthritis. *Arthritis Rheum, 62*(2), 463-471. doi:10.1002/art.27202

Simon, J., Surber, R., Kleinstauber, G., Petrow, P. K., Henzgen, S., Kinne, R. W., & Brauer, R. (2001). Systemic macrophage activation in locally-induced experimental arthritis. *J Autoimmun, 17*(2), 127-136. doi:10.1006/jaut.2001.0534

Singh, J. A., Noorbaloochi, S., & Knutson, K. L. (2017). Cytokine and neuropeptide levels are associated with pain relief in patients with chronically painful total knee arthroplasty: a pilot study. *BMC Musculoskelet Disord, 18*(1), 17. doi:10.1186/s12891-016-1375-2

Smith, S., & Vale, W. (2016). The role of the hypothalamic-pituitary-adrenal axis in neuroendocrine responses to stress. *Dialogues Clin Neuroscience, 8*.

Steinbach, E. C., & Plevy, S. E. (2014). The role of macrophages and dendritic cells in the initiation of inflammation in IBD. *Inflamm Bowel Dis, 20*(1), 166-175. doi:10.1097/MIB.0b013e3182a69dca

Stewart, A. M., Roy, S., Wong, K., Gaikwad, S., Chung, K. M., & Kalueff, A. V. (2015). Cytokine and endocrine parameters in mouse chronic social defeat: implications for translational 'cross-domain' modeling of stress-related brain disorders. *Behav Brain Res, 276*, 84-91. doi:10.1016/j.bbr.2014.08.037

Stewart, H. L., & Kawcak, C. E. (2018). The Importance of Subchondral Bone in the Pathophysiology of Osteoarthritis. *Front Vet Sci, 5*, 178. doi:10.3389/fvets.2018.00178

Tarride, J. E., Haq, M., O'Reilly, D. J., Bowen, J. M., Xie, F., Dolovich, L., & Goeree, R. (2012). The excess burden of osteoarthritis in the province of Ontario, Canada. *Arthritis Rheum, 64*(4), 1153-1161. doi:10.1002/art.33467

Thodeti, C. K., Paruchuri, S., & Meszaros, J. G. (2013). A TRP to cardiac fibroblast differentiation. *Channels (Austin), 7*(3), 211-214. doi:10.4161/chan.24328

Toyoda, A. (2017). Social defeat models in animal science: What we have learned from rodent models. *Anim Sci J, 88*(7), 944-952. doi:10.1111/asj.12809

Vavken, P., & Dorotka, R. (2011). Burden of musculoskeletal disease and its determination by urbanicity, socioeconomic status, age, and sex: Results from 14,507 subjects. *Arthritis Care Res (Hoboken), 63*(11), 1558-1564. doi:10.1002/acr.20558

Viana, F. (2016). TRPA1 channels: molecular sentinels of cellular stress and tissue damage. *J Physiol, 594*(15), 4151-4169. doi:10.1113/JP270935

Vina, E. R., & Kwoh, C. K. (2018). Epidemiology of osteoarthritis: literature update. *Curr Opin Rheumatol, 30*(2), 160-167. doi:10.1097/BOR.0000000000000479

Volkers, L., Mechioukhi, Y., & Coste, B. (2015). Piezo channels: from structure to function. *Pflugers Arch, 467*(1), 95-99. doi:10.1007/s00424-014-1578-z

Wang, S., Kobayashi, K., Kogure, Y., Yamanaka, H., Yamamoto, S., Yagi, H., . . . Dai, Y. (2018). Negative Regulation of TRPA1 by AMPK in Primary Sensory Neurons as a Potential Mechanism of Painful Diabetic Neuropathy. *Diabetes, 67*(1), 98-109. doi:10.2337/db17-0503

Watari, T., Naito, K., Sakamoto, K., Kurosawa, H., Nagaoaka, I., & Kaneko, K. (2011). Evaluation of the effect of oxidative stress on articular cartilage in spontaneously osteoarthritic STR/OrtCrlj mice by measuring the biomarkers for oxidative stress and type II collagen degradation/synthesis. *Experimental and Therapeutic Medicine, 2*, 245-250.

Wilkinson, L., Pitsillides, A., Worrall, J., & Edwards, J. (1992). Light Microscopic Characterization of the Fibroblast-Like Synovial Intimal Cell (Synoviocyte). *Arthritis and Rheumatism, 35*(10).

Wu, J., Lewis, A. H., & Grandl, J. (2017). Touch, Tension, and Transduction - The Function and Regulation of Piezo Ion Channels. *Trends Biochem Sci, 42*(1), 57-71. doi:10.1016/j.tibs.2016.09.004

Xing, J., & Li, J. (2017). TRPA1 Function in Skeletal Muscle Sensory Neurons Following Femoral Artery Occlusion. *Cell Physiol Biochem, 42*(6), 2307-2317. doi:10.1159/000480003

Yerramilli, M., Farace, G., Quinn, J., & Yerramilli, M. (2016). Kidney Disease and the Nexus of Chronic Kidney Disease and Acute Kidney Injury: The Role of Novel Biomarkers as Early and Accurate Diagnostics. *Vet Clin North Am Small Anim Pract, 46*(6), 961-993. doi:10.1016/j.cvsm.2016.06.011

Yu, X. W., Hu, Z. L., Ni, M., Fang, P., Zhang, P. W., Shu, Q., . . . Wang, F. (2015). Acid-sensing ion channels promote the inflammation and migration of cultured rat microglia. *Glia, 63*(3), 483-496. doi:10.1002/glia.22766

Zhao, R., & Tsang, S. Y. (2017). Versatile Roles of Intracellularly Located TRPV1 Channel. *J Cell Physiol, 232*(8), 1957-1965. doi:10.1002/jcp.25704

Zheng, J. (2013). Molecular mechanism of TRP channels. *Compr Physiol, 3*(1), 221-242. doi:10.1002/cphy.c120001